Numerical investigation of harbor oscillations induced by focused transient wave groups

Junliang Gao [a, b, c], Xiaozhou Ma [b *], Jun Zang [c], Guohai Dong [b], Xiaojian Ma [a], Yazhou Zhu [a], Li Zhou [a]

[a] School of Naval Architecture and Ocean Engineering, Jiangsu University of Science and Technology, Zhenjiang 212003, China.

[b] State Key Laboratory of Coastal and Offshore Engineering, Dalian University of Technology, Dalian 116024, China.

[c] Research Unit for Water, Environment and Infrastructure Resilience (WEIR), Department of Architecture and Civil Engineering, University of Bath, BA2 7AY, U.K.

Abstract:

Focused wave groups are traveling waves characterized by extremely-large transient wave amplitudes and very short durations. These waves usually cause serious damage to marine/offshore structures and coastal infrastructures, and can even result in human casualties (Nikolkina and Didenkulova, 2011). The studies on natural disasters related to the focused wave groups near the coastal zone have been mostly confined to wave evolution over beaches, wave runup, overtopping, and their impact forces acting on the coastal infrastructures (e.g., the seawall and the circular cylinder); the influence of focused transient wave groups on harbors has not yet been studied.

In this study, the generation and propagation of focused transient wave groups and their interactions with the harbor are simulated using a fully nonlinear Boussinesq model, FUNWAVE 2.0. To this end, four elongated harbors with constant depth and a series of focused wave groups with various focused wave amplitudes, spectral width parameters, and incident directions are considered. Based on the Morlet wavelet transform and discrete Fourier transform techniques, the capability of focused transient wave groups to trigger the harbor resonance phenomenon is revealed for the first time. Subsequently, the influences of spectral width parameter, incident wave direction, and resonant mode on different resonant wave parameters (including maximum runup and resonant intensity of various resonant modes inside a harbor) are comprehensively investigated, and it is

*Corresponding author. E-mail address: maxzh@dlut.edu.cn.

found that these three factors have significant effects on resonant wave parameters.

Keywords:

Harbor resonance; Harbor oscillations; Focused transient wave groups; Maximum runup; Resonant intensity; Boussinesq model

1. Introduction

Harbor resonance (also termed as *harbor oscillations*) is the trapping and amplification of wave energy inside a semi-enclosed water body, such as a bay or harbor. It may be induced by infragravity waves, steady-state wave groups, atmospheric fluctuations, tsunami waves, or shear flows traveling into the semi-enclosed water body (Bowers, 1977; De Jong and Battjes, 2004; Dong et al., 2013; Fabrikant, 1995; Gao et al., 2017a; Gao et al., 2019a; Gao et al., 2019b; Kumar and Gulshan, 2017; Okihiro and Guza, 1996). Harbor oscillations may interrupt the operation of docks and create excessive mooring forces that probably break mooring lines by generating unacceptable vessel movements (Gulshan et al., 2020; Kumar et al., 2016; López and Iglesias, 2014). The early stage developments and the recent advances in understanding and modelling of harbor resonance had been reviewed by Miles (1974) and Rabinovich (2009), respectively.

The scientific studies on harbor resonance began in the early 1950s (Vanoni and Carr, 1950); however, the overwhelming majority of past investigations were restricted to stationary or transient harbor resonance induced by external oceanic waves propagating from the open sea. The stationary harbor resonance is mainly triggered by periodic forcing waves, such as steady-state short wave groups or steady-state infragravity waves. The resonance inside a harbor increases considerably before the energy input from the external oceanic waves is balanced by energy losses caused by boundary absorption, bottom friction, and radiation from the entrance (e.g., Chen et al. (2006); Gao et al. (2017b); Gao et al. (2018b); Kumar and Gulshan (2018); Losada et al. (2008); Rupali et al. (2020); Wang et al. (2011); Wang et al. (2014)). The transient resonance inside a harbor is mainly triggered by transient long waves, such as various types of tsunami waves including solitary waves, N-waves, and successive solitary waves (Dong et al., 2010a; Gao et al., 2018a). When the transient long waves impact on the harbor, the resonance does not experience a prolonged growth stage and immediately attains its maximum value (Dong et al., 2010a).

In the field of marine/offshore engineering, a compact focused wave group, which is referred to as NewWave for design purposes, was proposed by Tromans et al. (1991). Based on the rigorous probabilistic analysis of the local maximum shapes for linear Gaussian processes (Lindgren, 1970), the expected shape of a large wave in a sea state is successfully linked to the bulk properties of the sea state by the NewWave theory. This theory provides an efficient alternative to either long regular wave or irregular wave design methods for scientific and engineering issues wherein the survivability of structures subjected to extreme events or the overtopping over structures are the primary concerns. In particular, an extreme response during a specified period of irregular wave incidence could be reproduced accurately by using a short-time experiment (Jonathan and Taylor, 1997). In the last two decades, the related theories and applications of the focused wave groups have been significantly developed in marine/offshore engineering (e.g., Bredmose and Jacobsen (2010); Buldakov et al. (2003); Chen et al. (2018); Dong et al. (2019); Liu et al. (2015); Ma et al. (2009); Zhao et al. (2017)).

Although focused wave groups have been well established and widely utilized in marine/offshore engineering, their use in coastal engineering is still relatively rare and novel. Based on laboratory experiments, Hunt-Raby et al. (2011) investigated the overtopping of two types of extreme waves (focused wave groups and solitary waves) on a trapezoidal embankment. Paulsen et al. (2014) proposed a fully nonlinear domain-decomposed solver to efficiently compute the wave loads on the surface-piercing circular cylinder. Four different incident wave trains with increasing complexity including the focused wave groups were considered. Subsequently, by coupling a higher-order boundary element method with a mixed Eulerian–Lagrangian technique, Ning et al. (2017) extensively studied the runup of focused wave groups and their pressure on a vertical seawall. Recently, both laboratory measurements and numerical simulations of multi-directional focused wave groups interacting with a plane beach were presented by Judge et al. (2019). The adopted numerical model was a hybrid flow solver governed by a Boussinesq equation set for pre-breaking and nonlinear shallow water equations for post-breaking, and the wave evolution processes and the extreme runup on the beach were systematically investigated.

As can be seen from the descriptions in the previous paragraph, heretofore, the studies on natural disasters triggered by focused wave groups in coastal zones have been mostly confined to wave evolution over the beach, wave runup, overtopping, and their impact forces acting on the

coastal infrastructures (e.g., the seawall and the circular cylinder). To the best of our knowledge, the interactions between focused transient wave groups and harbors have not yet been investigated. The stationary harbor resonance induced by steady-state wave groups has been extensively investigated by many scholars (e.g., Bowers (1977); Chen et al. (2006)). For the stationary harbor resonance, a relatively long time is required to trap and amplify the wave energy of various resonant modes inside the harbor (Bellotti, 2007; Dong et al., 2010b; Gao et al., 2016). However, focused wave groups have the transient nature. Sufficient time is not available for them to trap and amplify the wave energy of various resonant modes inside the harbor. Therefore, the following three questions arise:
(1) Can focused wave groups trigger the harbor resonance phenomenon under certain circumstances?
(2) If the answer to question (1) is yes, how the variation of incident wave parameters, such as spectral width parameter and incident wave direction, will affect the resonant wave surfaces inside the harbor?
(3) If the answer to question (1) is yes, what are the differences between the resonant responses of various modes when they are triggered by an identical focused wave group?

To address these questions, in this study, we systematically investigate focused wave group interactions with four different harbors for the first time. The generation and propagation of focused wave groups and their interactions with the harbor are implemented by employing the fully nonlinear Boussinesq equation model, FUNWAVE 2.0 (Kirby et al., 2003). A series of focused transient wave groups with identical spectral peak frequency and different spectral width parameters, and focused wave amplitudes are generated. To create the desired focused transient wave groups, the NewWave theory and an amplitude/phase iterative technique are first adopted in a simple elongated wave flume in the absence of the harbor. Once the desired wave trains are obtained, their wave-making signals are then used as the input parameters in other two wave flumes, which have different harbor layouts, so that the incident focused wave groups can travel into the harbor from two different directions (perpendicularly to or parallel with the harbor entrance). For simplification, all the four harbors are assumed to be long and narrow; the free-surface displacement inside them essentially becomes one-dimensional. The water depth inside and outside the harbors is set to a constant. To record the wave surfaces triggered by the incident focused wave trains, a series of numerical wave gauges are deployed inside the harbors.

Morlet wavelet transform (MWT) and discrete Fourier transform (DFT) techniques are adopted

to check both the time- and frequency-domain information of the wave surfaces inside the harbor, through which the capacity of the focused wave groups to trigger the harbor resonance phenomenon is first revealed in this study. Further, the influences of two incident wave parameters (spectral width parameter and incident wave direction) and different resonant modes on resonant wave parameters inside the harbor are extensively studied. The following two resonant wave parameters are concerned: (i) the maximum runup inside the harbor, which is closely related to the wave-induced overtopping and inundation, and (ii) the resonant intensity of various resonant modes, which significantly affects the motion of the ships moored inside the harbor, and thus, is closely associated with the port's operational efficiency.

The remainder of the paper is organized as follows: Section 2 introduces the numerical model and the data analysis technique. The capacity of the former to accurately reproduce the harbor oscillations induced by incident waves with different incident angles is validated by two laboratory experiments. Section 3 describes the generation methods of focused transient wave groups, which include the NewWave theory and the amplitude/phase iterative technique, and presents the setup of the numerical wave flume as well. Section 4 describes the simulation results along with detailed explanations. Concluding remarks based on the results are given in Section 5.

2. Numerical model and data analysis technique

2.1. Numerical model description

In this study, numerical simulations are implemented by adopting the well-known and widely-used FUNWAVE 2.0 model (Kirby et al., 2003), which refers to a fully nonlinear Boussinesq wave model in the generalized curvilinear coordinates. FUNWAVE 2.0 was initially developed by the research group at Center for Applied Coastal Research of University of Delaware. This model solves a set of fully nonlinear Boussinesq equations of Wei et al. (1995) using a finite difference scheme and merges a moving reference level as done in a study by Kennedy et al. (2001). With the advances in both nonlinearity and dispersion, the numerical model is able to accurately simulate the propagation and transformation of the oceanic waves with strong nonlinearity in two horizontal-dimensions from intermediate depth to zero water depth (Bruno et al., 2009; Kirby et al., 2003). The one-way wave maker theory proposed by Chawla and Kirby (2000) is used to generate monochromatic or random waves, and the line source wave-making method proposed by Lee et al.

(2001) is adopted to create focused transient wave groups in the present work. Sponge layers are deployed at the boundaries of the numerical wave flume to effectively absorb the outgoing waves with various directions and frequencies.

2.2. Numerical model verification by physical experiment

Considering that the influence of the incident direction of focused wave groups on the harbor resonance is one of the main concerns in this study, the capacity of FUNWAVE 2.0 to simulate harbor resonance excited by incident waves with different incident angles is first validated in this section. The numerical model is used to reproduce harbor resonance experiments of Losada et al. (2008) and De Girolamo (1996), wherein the harbor resonance induced by normally-incident regular waves with various wave heights and that excited by parallel-incident wave groups with various frequency components were implemented, respectively. The time series of the resonant free-surface elevations inside the harbor and the amplification factor curves of the wave surfaces inside the harbor predicted by the numerical model are compared with the experimental measurements of these two studies, respectively.

2.2.1 Harbor oscillations excited by normally-incident waves

To deepen the understanding on the process of nonlinear harbor oscillations and to validate their numerical model, a series of laboratory experiments of harbor resonance inside two adjacent parallel rectangular narrow inlets with variable lengths were implemented by Losada et al. (2008) in a 70 m long, 2 m wide and 2 m high wave flume at the University of Cantabria. The flume is equipped with a wave generation system composed of a pendulum type wave maker and an active wave absorption control system.

Fig. 1 shows the experimental setup and locations of wave gauges for the experiments of Losada et al. (2008). The physical model consisted of two adjacent narrow rectangular inlets positioned at the right end of the wave flume. The width of the two inlets was set to a constant value of 0.2 m and their lengths varied between 0 and 5 m. The longitudinal axis of Inlet 1 was deployed at the center of the flume, and that of Inlet 2 was 0.5 m off and closer to one of the flume lateral walls. The entrance position of both inlets remained unchanged throughout the experiments. A total of 25 sub-geometries were obtained by combining five different fixed lengths for Inlet 1 (L_1=1, 2,

3, 4, and 5 m) with five fractional lengths (0, 0.25, 0.5, 0.75, and 1) for Inlet 2, among which the lengths of 1, 3, and 5 m match the natural resonant mode for the experimental wave conditions. Regular wave trains with various wave heights and a constant wave period of T=2 s were generated and propagated from left to right of the wave flume (the direction of the incident waves is perpendicular to the inlet entrance). The water depth was constant, h=0.5 m, thereby yielding a wavelength of L=4.06 m. The time series of free-surface elevations were measured at 18 locations inside the wave flume.

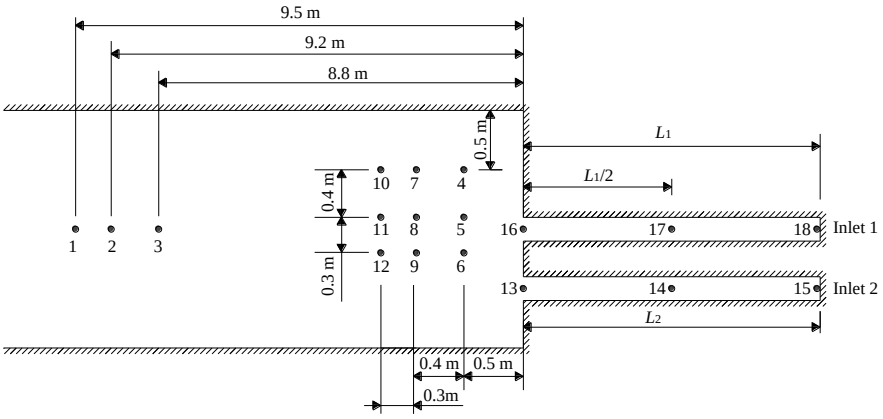

Fig. 1. Definition sketch of the experimental setup and the locations of wave gauges for the experiments of Losada et al. (2008).

In this section, four cases of the experiments of Losada et al. (2008) are chosen to be reproduced by FUNWAVE 2.0, and the experimental parameters for these cases are listed in Table 1. For cases 0101 and 0303, the entrance of Inlet 2 is closed (L_2=0) and the 1st and the 2nd resonant modes of Inlet 1 are excited by the incident regular waves, respectively. For cases 0903 and 1702, the two inlets have the identical lengths, and the 3rd and the 2nd modes of both inlets are induced by the waves, respectively. In addition, the resonance of water bodies inside them will interact with each other because of the close distance between the entrances of the two inlets, which is called as "coupled oscillations" (Liu et al., 2003; Marcos et al., 2004). The numerical wave flume used for reproducing the physical experiments is presented in Fig. 2. Compared to the physical wave flume, the length of the numerical flume is significantly reduced because the sponge layer deployed near the left boundary absorbs the reflecting waves effectively. As the numerical model is discretized

using curvilinear grids, different grid spaces are used. In the *x*-direction, for the domain where there is no sponge layer deployed (hereinafter referred to as "no-sponge-layer domain"), the grid size Δx is set to a constant value of 0.05 m; however, for the sponge-layer domain, Δx, increases gradually from 0.05 to 0.30 m. In the *y*-direction, the grid size Δy is kept at a constant value of 0.025 m. The time step of Δt=0.005 s is adopted for all these simulations.

Table 1. Experimental parameters for part of the experiments of Losada et al. (2008)

Case	L_1 (m)	L_2 (m)	H (m)	$\varepsilon=H/L$
0101	1.0	0.0	0.05	0.0123
0303	3.0	0.0	0.05	0.0123
0903	5.0	5.0	0.05	0.0123
1702	3.0	3.0	0.025	0.0061

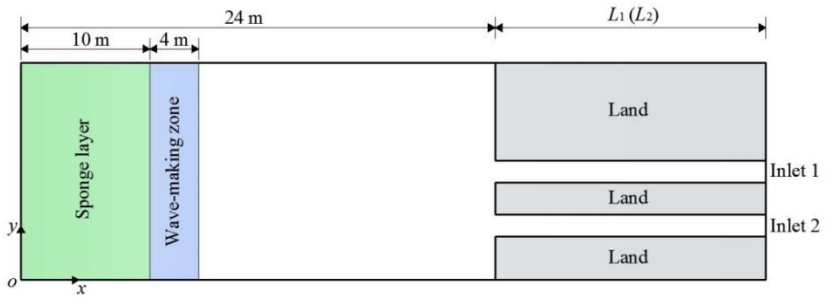

Fig. 2. Sketch of the numerical flume for the experiments of Losada et al. (2008).

Fig. 3 illustrates the measured and model-predicted time series of the free-surface elevations at gauges G_{18} and G_{15} for the four cases listed in Table 1. It is observed that the measured data and the numerical results for all the four cases are in good agreement. All nonlinear characteristics, such as asymmetry of waveform and occurrence of secondary crests, are captured accurately by the FUNWAVE 2.0 model.

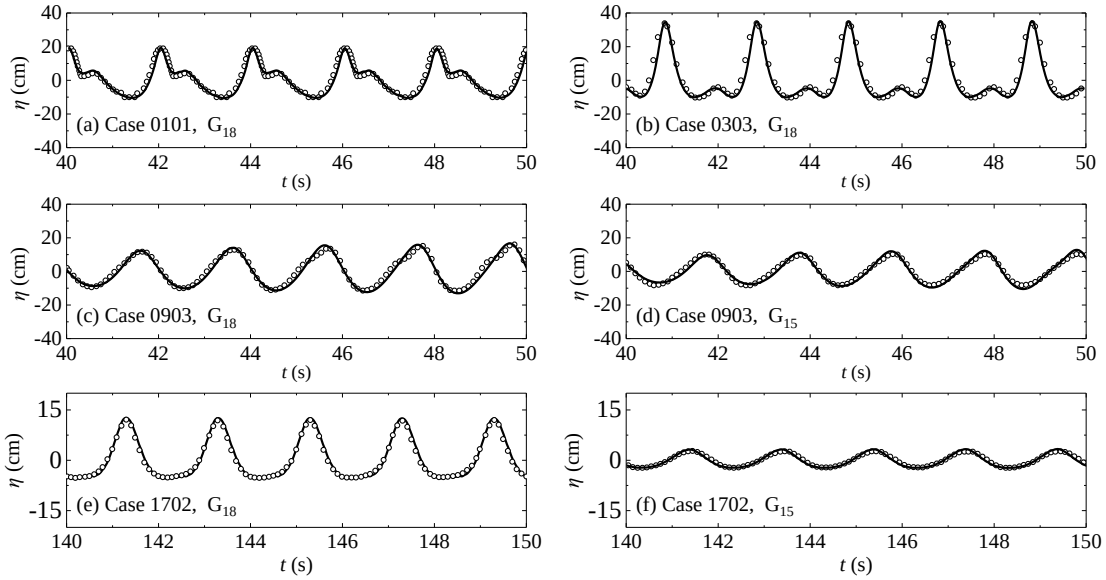

Fig. 3. Comparisons of the time series of the numerical (line) and experimental (dot) free surfaces at gauges G_{18} and G_{15} for the four cases listed in Table 1.

2.2.2 Harbor oscillations excited by parallel-incident waves

To determine if there are differences in the harbor response when oscillations are excited by regular free long waves or by bound long waves, De Girolamo (1996) performed a set of laboratory experiments to model the harbor resonance induced by regular long waves, bichromatic short-wave groups, and irregular short waves. The physical model was composed of a 15 m long and 3 m wide wave flume connected to a square basin (16 m × 16 m). A piston-type wave generator was deployed at the upstream end of the wave flume. One side of the flume outlet was made by a vertical wall of a sector of circle with the radius of 2 m. A narrow bay was arranged inside the square basin with its main axis being orthogonal to the straight vertical wall of the flume, which means that the direction of the incident waves is parallel to the bay entrance. Two bays with the same width and different lengths were considered: the longer one with the length of 2.4 m (Bay A) and the shorter one with the length of 1.2 m (Bay B). Both of them have the width of 0.2 m. The bottom of the bay, of the wave flume and of part of the basin was a horizontal, smooth concrete surface. The remaining part of the horizontal basin bottom was covered with gravel. The still water depth over the horizontal bottom was set to 0.15 m. Gravel beaches were arranged around the boundaries of the basin to efficiently absorb the outgoing wave energy.

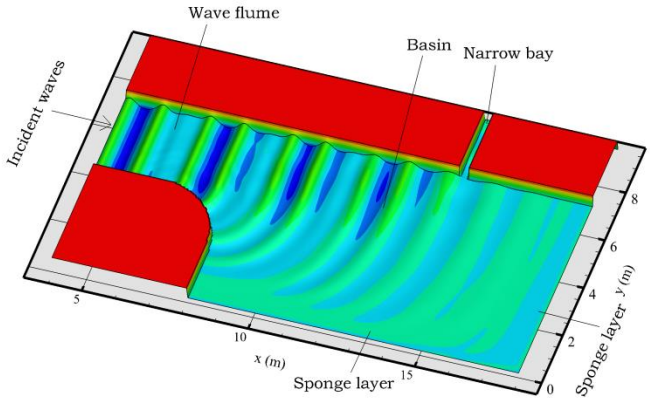

Fig. 4. Reproduction of the experimental set-up of De Girolamo (1996).

Fig. 4 shows the reproduction of the experimental setup in the numerical simulations. In this study, only the bay responses excited by bichromatic wave groups are simulated. The bichromatic short-wave groups were gained by using two regular short-wave components with slightly different frequencies, ω_1 and ω_2, so that wave groups occurred at a beat frequency $\Delta\omega = \omega_2 - \omega_1$ (assuming $\omega_2 > \omega_1$). In De Girolamo (1996), the frequency ω_1 was kept constant, i.e., $\omega_1 \equiv 5.71$ rad/s, and ω_2 was modified to obtain beat frequencies around the peak frequencies of the amplification diagram gained experimentally by using regular long waves. The amplitude of the short-wave components was about 1 cm for all the tests. Non-uniform grid sizes are adopted in both the *x*- and *y*-directions. In the *x*-direction, the grid size Δx is set to a constant value of 0.06 m in the area of the wave flume where the incident waves are generated and propagates toward the basin. Subsequently, Δx gradually decreases from 0.06 m at the outlet of the wave flume to 0.02 m near and at the bay entrance. Further, Δx increases gradually from 0.02 m at the beginning of the right sponge layer to 0.32 m at the right boundary. In the *y*-direction, the grid size Δy is kept a constant value of 0.02 m inside the bay and then increases gradually from 0.02 m at the bay entrance to 0.34 m at the lower boundary of the numerical wave flume. The time step of Δt=0.008 s is adopted.

Fig. 5 presents the comparison between the model-predicted and the measured amplification factor *F*, which is defined as

$$F(\omega) = \sqrt{\frac{S_0(\Delta\omega)}{S_C(\Delta\omega) + \delta}} \,. \tag{1}$$

$S_0(\Delta\omega)$ and $S_C(\Delta\omega)$ are the energy spectrum densities measured at the backwall of the bay with the bay entrance open and that measured in front of the bay with the entrance closed, respectively;

δ is a constant small finite quantity (δ=0.03 cm^2 s/rad). It is observed that for both Bay A and Bay B, the model-predicted amplification factors present good consistency with the measurements overall, although the former is shown to be slightly larger than the latter. The maximum amplification factors obtained by the experiments are F=4.2 and F=2.1 for Bays A and B, respectively, and the corresponding numerical results are F=4.8 and F=2.6. The predicted results are slightly larger than the measured data because some wave energy dissipation mechanisms occur in the physical experiments, such as bottom friction and flow separation around the bay entrance, which are not considered in the numerical simulations.

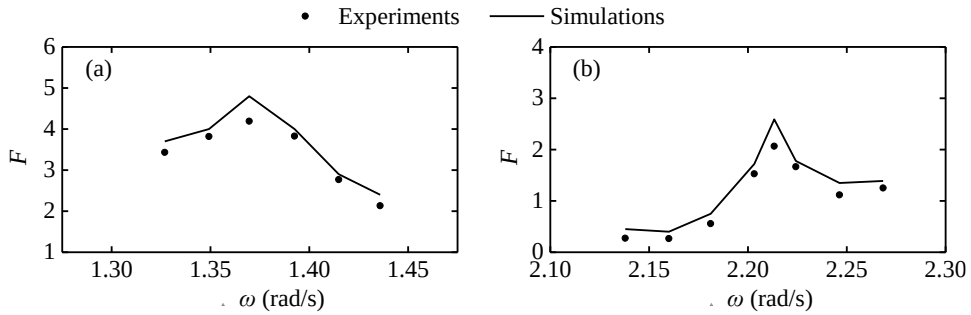

Fig. 5. Variation of amplification factor F related to the frequency of wave groups, $\Delta\omega$: (a) Bay A and (b) Bay B.

2.3. Data analysis technique

The simulation results for all numerical experiments conducted in this study will be analyzed by using the MWT and DFT techniques. Compared with the conventional Fourier transform, the wavelet transform technique is relatively new for signal processing. By featuring no assumption of stationary signal, the wavelet transform can create not only the localized frequency-domain information but also the localized time-domain information from the time series. For real time series, their analytical signals at each frequency can be established by the MWT because the Morlet wavelet is an analytical wavelet (Goupillaud et al., 1984). Over the last two decades, the MWT technique has been widely used in ocean and coastal engineering (Dong et al., 2008; Huang, 2004; Judge et al., 2019). In this study, to examine whether the focused transient wave groups can induce harbor resonance, the MWT is first used to analyze the time series of the free-surface elevations inside the harbor. Based on the research finding that the focused transient wave groups can successfully excite

the harbor resonance (this will be discussed further in subsection 4.1), the DFT is further adopted to quantitatively extract the response amplitudes of various resonant modes at different positions inside the harbor. It should be noted that because of the transient property of the focused wave groups, the response amplitudes of various resonant modes calculated by the DFT represent their time-averaged response amplitudes in the time range of the analysis.

3. Numerical experimental setup

3.1. Generation of focused wave groups

A NewWave-type focused transient wave group is composed of numerous individual cosine wave components, which focus at a specific point in space and time (Tromans et al., 1991). Based on the linear wave theory, the free-surface elevation at any spatial position and any time for a uni-directional focused wave group is expressed as follows:

$$\eta(x,t)=\sum_{n=1}^{N} a_n \cos\varphi_n \,, \tag{2}$$

where

$$a_n = A_{\mathrm{f}} \frac{S(f_n)\times\Delta f}{\sum_{n=1}^{N} S(f_n)\times\Delta f}, \tag{3}$$

$$\varphi_n = k_n(x-x_{\mathrm{f}}) - 2\pi f_n (t-t_{\mathrm{f}}). \tag{4}$$

In the above equations, N denotes the number of all compositive wave components. a_n, f_n, and k_n denote the wave amplitude, frequency, and wavenumber of the n^{th} wave component, respectively, wherein f_n and k_n satisfy the following linear dispersion relationship:

$$(2\pi f_n)^2 = g k_n \tanh(k_n h). \tag{5}$$

A_{f} is the focused wave amplitude that occur at the focus location and time. x_{f} and t_{f} are the focus location and focus time, respectively. Δf is the frequency increment. $S(f_n)$ is the wave energy spectrum that describes the wave energy distribution among various wave components. In this study, the modified JONSWAP spectrum suggested by Goda (1999) is adopted, which is expressed as

$$S(f) = \beta_J H_{1/3}^2 T_p^{-4} f^{-5} \exp\left[-\frac{5}{4}(T_p f)^{-4}\right] \times \gamma^{\exp\left[-(f/f_p-1)^2/2\sigma^2\right]}, \tag{6}$$

where f is the frequency, σ is the spectral shape parameter, and $\sigma = 0.07$ when $f < 1/T_{\mathrm{p}}$, otherwise $\sigma = 0.09$. T_{p} is the spectral peak period, $f_{\mathrm{p}}=1/T_{\mathrm{p}}$ is the spectral peak frequency, and γ is the spectral

bandwidth parameter. β_J is defined as a function of the spectrum bandwidth parameter and is expressed as follows:

$$\beta_J = \frac{0.06238 \times [1.094 - 0.01915 \ln \gamma]}{0.23 + 0.0336\gamma - 0.185(1.9 + \gamma)^{-1}} . \quad (7)$$

In the current research, 100 frequency components equally spaced between $0.3f_p$ to $3.0f_p$ are utilized to generate the focused transient wave group.

It should be noted that the dispersive focusing method given in Eq. (2) is based on the linear wave theory, which would inevitably cause a shift of the actual focused position and focused amplitude because of nonlinear wave-wave interactions (Baldock et al., 1996; Johannessen and Swan, 2008). In this study, the iterative approach proposed by Schmittner et al. (2009) and Fernández et al. (2014) is adopted. The method iteratively corrects both the initial phases and the amplitudes of various frequency components in a wave group, which is given by

$$a_{\text{in}}^{k}(f_n) = a_{\text{in}}^{k-1}(f_n) a_{\text{tgt}}(f_n) / a_{\text{out}}^{k-1}(f_n) , \quad (8)$$

and

$$\varphi_{\text{in}}^{k}(f_n) = \varphi_{\text{in}}^{k-1}(f_n) + \left(\varphi_{\text{tgt}}(f_n) - \varphi_{\text{out}}^{k-1}(f_n)\right) , \quad (9)$$

where $a_{\text{in}}^{k}(f_n)$ and $\varphi_{\text{in}}^{k}(f_n)$ denote the amplitude and phase of an input spectral component at frequency f_n, respectively. $a_{\text{out}}^{k}(f_n)$ and $\varphi_{\text{out}}^{k}(f_n)$ denote the amplitude and phase of the corresponding frequency components of the recorded/measured output spectrum, respectively. The superscript k refers to the k^{th} iteration. $a_{\text{tgt}}(f_n)$ and $\varphi_{\text{tgt}}(f_n)$ are determined by the pre-selected target spectrum, i.e., Eq. (6). Iteration continues until the simulated focused wave amplitude matches the target one, and various frequency components focus at the desired location in the flume.

3.2. Numerical wave flume

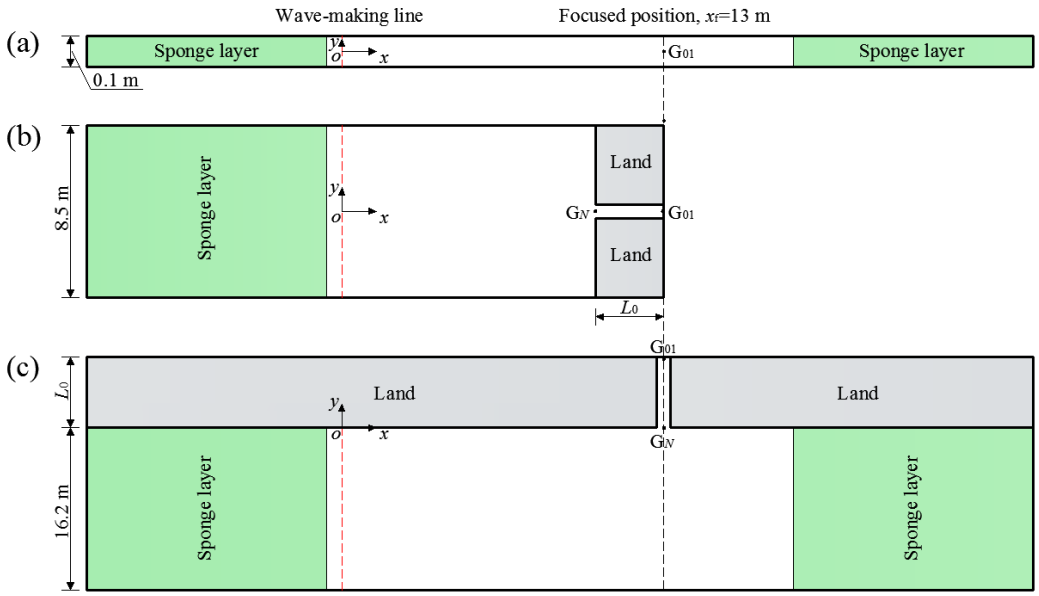

Fig. 6. Numerical wave flumes and the definition of the coordinate systems for generating focused wave groups (a) without harbor, (b) vertically propagating into the harbor, and (c) parallel propagating into the harbor. The red and black dashed lines refer to the wave-making lines and the target focused position, respectively. L_0 denotes the length of the harbor.

Fig. 6 shows the three numerical wave flumes adopted in all the simulations and the definition of their coordinate systems. To generate the desired focused transient wave groups, a simple elongated wave flume in the absence of the harbor is first utilized (Fig. 6a). The origin of the coordinate system for each numerical wave flume is always defined at the wave-making line. The target focused position is always set to x_f =13.0 m for all focused wave groups considered in this article. Based on the NewWave theory and the amplitude/phase iterative method described in subsection 3.1, the desired focused wave groups with various wave parameters can be successfully generated. Subsequently, the obtained wave-generating signals are further utilized in the numerical wave flumes shown in Fig. 6b and c, wherein the incident focused wave groups coming from the left to the right can propagate into the harbor perpendicularly to or parallel with the harbor entrance, respectively. To reasonably investigate the effects of the incident wave direction on the wave surfaces (especially on the maximum runup) inside the harbor, for the wave flume shown in Fig. 6b, the position of the backwall of the harbor is always set to be at the focus point, and for the wave flume shown in Fig. 6c, the central line of the harbor is set to be collinear with the latter. This arrangement can eliminate the influence of inconsistent relative positions between the focused point

and the backwall of the harbor on the research results.

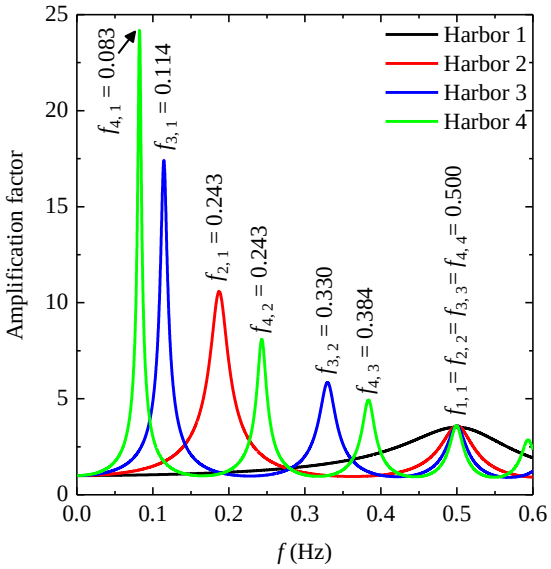

Fig. 7. Amplification factor curves of Harbors 1–4 predicted by using the linear analytical solution of Mei (1983). $f_{i,j}$ in the figure denotes the resonant frequency of the j^{th} mode (Mode j) for Harbor i.

In this paper, four elongated rectangular harbors with various lengths and identical width (Harbors 1–4) are considered. The lengths of Harbors 1–4, L_0, are set to 0.92, 3.56, 6.18, and 8.80 m, respectively, and their width is set to W=0.5 m. Based on the linear analytical solution for the resonance of an elongated harbor (Mei, 1983), the amplification factor curves of the four harbors are calculated and presented in Fig. 7. The symbol $f_{i,j}$ in the figure denotes the resonant frequency of the j^{th} mode (i.e. Mode j) for Harbor i (i=1, 2, 3, and 4). It is noted that for Mode 1 of Harbor 1, Mode 2 of Harbor 2, Mode 3 of Harbor 3 and Mode 4 of Harbor 4, they have the same resonant frequency and have almost the same linear amplification factor. Their resonant frequency is $f_{1,1}$ = $f_{2,2}$ = $f_{3,3}$ = $f_{4,4}$ = 0.50 Hz and their amplification factors are 3.54, 3.58, 3.59, and 3.60, respectively. To examine whether the focused wave groups can induce harbor resonance, the spectral peak frequency, f_p, of all the focused transient wave groups used in this study is set to equal the resonant frequency of these four modes, i.e., f_p = 0.50 Hz. The purpose of ensuring the same resonant frequency and the almost identical amplification factor for Mode 1 of Harbor 1, Mode 2 of Harbor 2, Mode 3 of Harbor 3 and Mode 4 of Harbor 4 is to better investigate the effects of different resonant modes on the wave surfaces inside the harbor (this will be discussed in subsection 4.4). In other words, the above experimental settings can eliminate the influences of inconsistent spectral peak

frequencies of the incident focused waves and inconsistent amplification factors on the research results. The focused wave amplitude, A_f, increases gradually from 0.02 m to 0.12 m, in an interval of 0.02 m. To reveal the effects of the spectral width parameter on harbor resonance, three different values of γ (i.e., γ = 1.3, 3.3 and 10) are considered.

For all the three numerical wave flumes shown in Fig. 6, all boundaries are set to be fully reflective vertical walls, the water depth is set to a constant of h=1.0 m, and the widths of the sponge layers deployed are all set to 30.0 m, which is approximately six times of the spectral peak wavelength L_p. The dimensions of the three wave flumes are 80.0 m × 0.1 m, 44.0 m × 8.5 m, and 80.0 m × (16.2+L_0) m (L_0 is the length of the harbor), respectively. For the wave flume shown in Fig. 6a, a wave gauge G_{01} is installed at x_f = 13.0 m to measure the time series of the free-surface elevation at the target focused position. In addition, to record the wave conditions inside the harbor, a series of wave gauges (G_{01}–G_N) are arranged equidistantly along the central line of the harbor, and the distance between adjacent wave gauges is always set to 0.1 m. The numbers of the wave gauges deployed inside Harbors 1–4, N, are 10, 36, 62, and 89, respectively. The gauge G_{01} is installed at the backwall of the harbor and the gauge G_N is near or just at the harbor entrance.

Non-uniform grid sizes are also utilized in the x-direction for all the three numerical wave flumes shown in Fig. 6. For the no-sponge-layer domains, the grid size Δx is set to a constant 0.025 m; however, for the sponge-layer domains, Δx gradually increases from 0.025 m to 0.628 m at the left/right boundaries. In the y-direction, for the two numerical flumes shown in Fig. 6a and b, the grid size Δy is kept at a constant value of 0.025 m in the whole computational domains; meanwhile, for the numerical flume shown in Fig. 6c, Δy is set to 0.025 m inside the harbor and then increases gradually from 0.025 m at the harbor entrance to 0.312 m at the lower boundary. For all the numerical experiments described in this section, a time step of Δt = 0.004 s is utilized, and the total simulation time is 65.0 s.

Prior to implementing numerical simulations, it is essential to check first whether the numerical model and the iterative approach described by Eqs. (8) and (9) can produce the desired focused wave groups accurately. Figs. 8 and 9 show the comparisons of the simulated and theoretical free-surface elevations and their amplitude spectra at the target focused position for the focused transient wave groups with A_f = 0.02 m and various spectral bandwidth parameters γ in the absence of the harbor, respectively. As shown in Fig. 8, the simulated free-surface elevations coincide fairly well

with the theoretical ones under the conditions of A_f = 0.02 m and various spectral bandwidth parameters. The good agreement between their amplitude spectra is also clearly observed in Fig. 9. This indicates that the FUNWAVE 2.0 model combined with the iterative approach has the capability to accurately generate the desired focused transient wave groups.

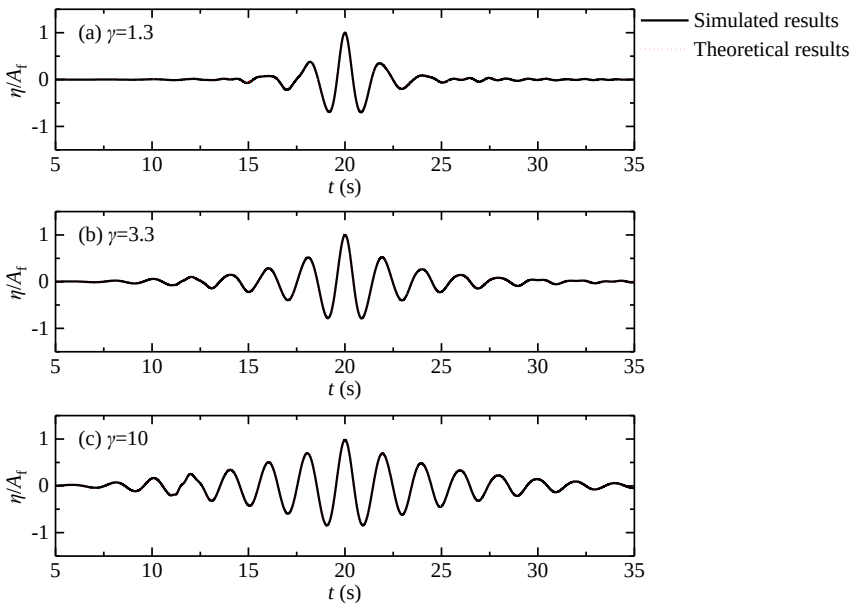

Fig. 8. Comparison of the simulated and theoretical free-surface elevations at the target focused position (i.e., at gauge G_{01}) for A_f = 0.02 m and various spectral bandwidth parameters γ in the absence of the harbor.

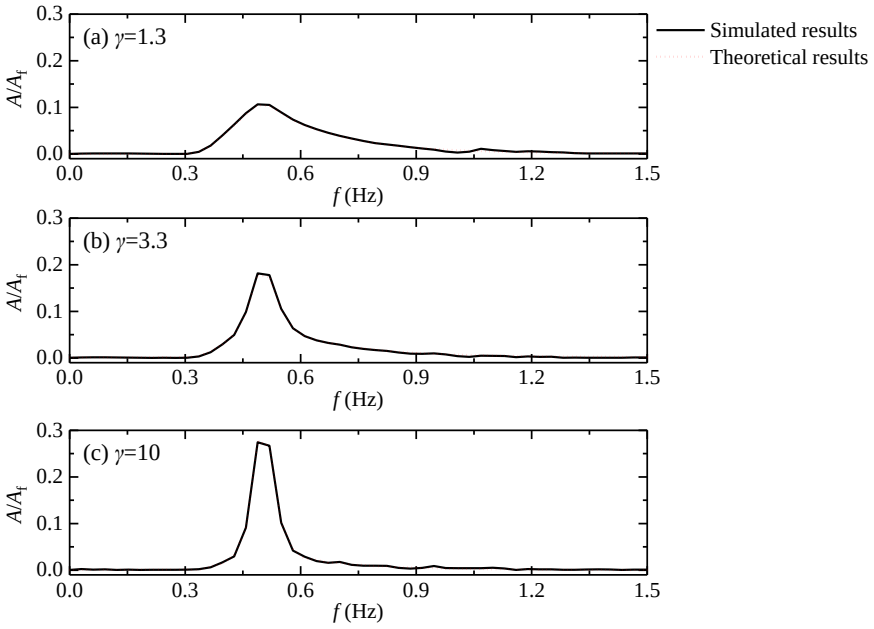

Fig. 9. Comparison of the simulated and theoretical amplitude spectra for the free-surface elevations shown in Fig. 8.

4. Results and discussion

The wave surfaces inside different harbors subjected to the focused wave groups with various values of γ in Eq. (6) are first analyzed in subsection 4.1 using both the MWT and DFT techniques, through which the capability of the focused wave groups to trigger the harbor oscillation phenomenon is revealed for the first time. Based on the analysis results in subsection 4.1, effects of the spectral width parameter γ, the incident wave direction and the resonant mode on resonant wave parameters inside the harbor are further investigated in subsections 4.2–4.4, respectively. The resonant wave parameters to be studied include the maximum runup inside the harbor and the response amplitude of various resonant modes. It should be noted that the term "the maximum runup inside the harbor" refers to the maximum vertically projected free-surface elevation inside the whole harbor. The maximum runup inside the harbor conceptually differs from the maximum free-surface elevation at the backwall of the harbor because the former may also occur at the sidewall of the harbor. However, for all the cases described in Section 3, the maximum runup inside the harbor is always equal to the maximum free-surface elevation at the backwall; this is established in subsection 4.1.

4.1. Time series and spectra analysis

Fig. 10 presents the spatial distributions of the maximum free-surface elevations inside Harbors 1–4 excited by focused wave groups with A_f = 0.12 m, γ=3.3 and different incident directions. R in this figure denotes the maximum free-surface elevation at each wave gauge. It is seen that for all the four harbors, the maximum runup inside the harbor always occurs at the backwall (at gauge G_{01}), regardless of whether the incident focused wave groups propagate into the harbor perpendicularly to or parallel with the harbor entrance. For other incident focused wave amplitudes and spectral-width parameters, the similar phenomenon can also be observed. Hence, it is proved that for all the cases considered, the maximum runup inside the harbor, A_u, is always equal to the maximum free-surface elevation at gauge G_{01}.

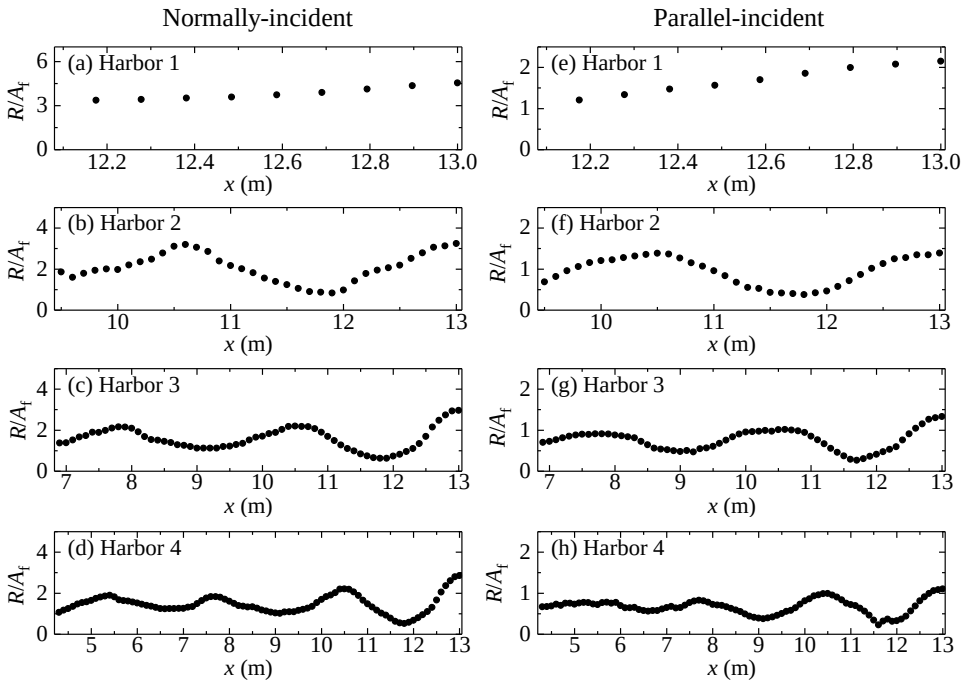

Fig. 10. Spatial distributions of the maximum free-surface elevations inside the harbor excited by focused wave groups with A_f = 0.12 m and γ=3.3. (a)–(d) correspond to Harbors 1–4 subjected to normally-incident focused wave groups, respectively. (e)–(h) correspond to Harbors 1–4 subjected to parallel-incident focused wave groups, respectively. The symbol R in this figure denotes the maximum free-surface elevation at each wave gauge.

Fig. 11 shows the comparisons of the time series of the free-surface elevation at gauge G_{01} in the absence of the harbor and the corresponding ones inside Harbors 1 and 4 excited by normally-incident focused wave groups with A_f = 0.12 m and various values of γ. Four obvious phenomena can be easily seen. First, due to the existence of the harbor, the maximum response amplitudes at gauge G_{01} inside both harbors are much larger than the focused amplitudes of the incident focused wave groups. The value of A_u/A_f varies between 2.65 and 6.09 for the six cases shown in this figure. Second, the maximum response amplitudes inside Harbor 1 are shown to be obviously larger than those inside Harbor 4 for all the three values of γ. Third, the maximum response amplitude inside both harbors increases gradually with the increase of γ. Fourth, compared to the incident focused wave groups, it takes much longer time for the wave surfaces inside both harbors to return to calm. Generally, for all the six cases in this figure, the incident focused wave groups have almost totally passed through the gauge G_{01} at t =35.0 s in the absence of the harbor; however, for the wave surfaces

inside both harbors, they always show obvious fluctuations until the end of the simulation.

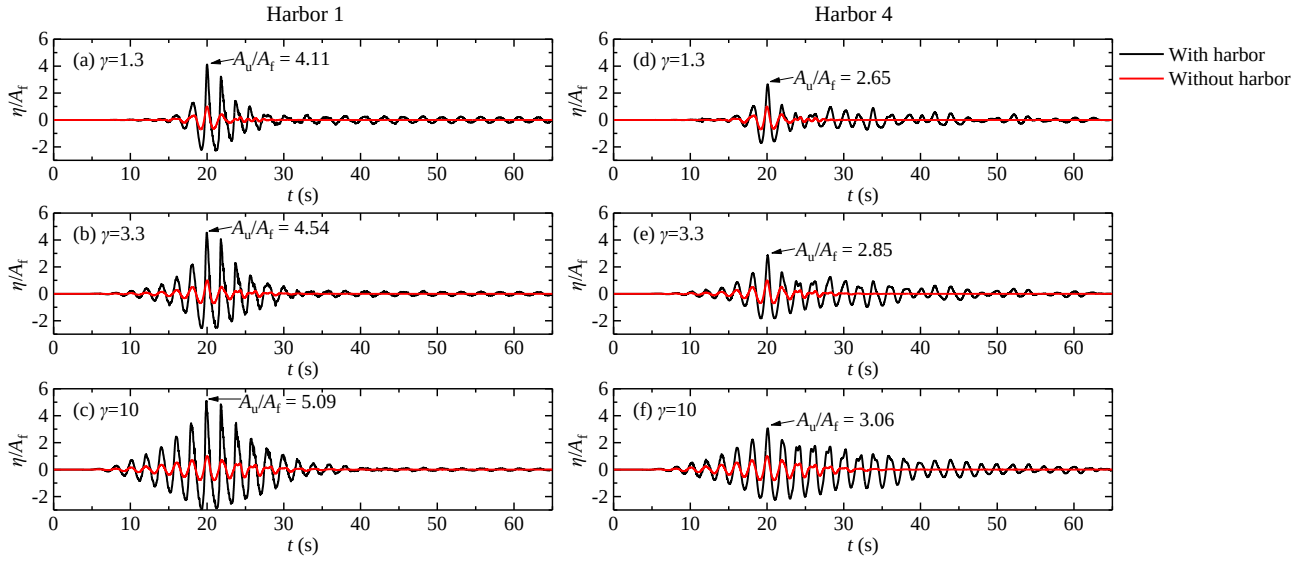

Fig. 11. Time series of the free-surface elevation at gauge G_{01} in the absence of the harbor and the corresponding ones inside Harbors 1 and 4 excited by normally-incident focused wave groups with A_f = 0.12 m and various values of γ. (a)–(c) and (d)–(f) correspond to Harbors 1 and 4, respectively. A_u denotes the maximum free-surface elevation at gauge G_{01} inside the harbor (i.e., the maximum runup inside the harbor).

It should be noted that the first and fourth phenomena described above coincide well with the following two typical characteristics of harbor oscillations: (i) the free-surface elevation inside the harbor can be remarkably amplified, and (ii) the resonant wave surfaces inside the harbor always need a long time to restore calm (Bellotti, 2007; Dong et al., 2010b). Therefore, it can be inferred that the focused transient wave groups are probably able to excite the significant harbor oscillations. The second and third phenomena will be discussed in detail in subsections 4.2 and 4.4.

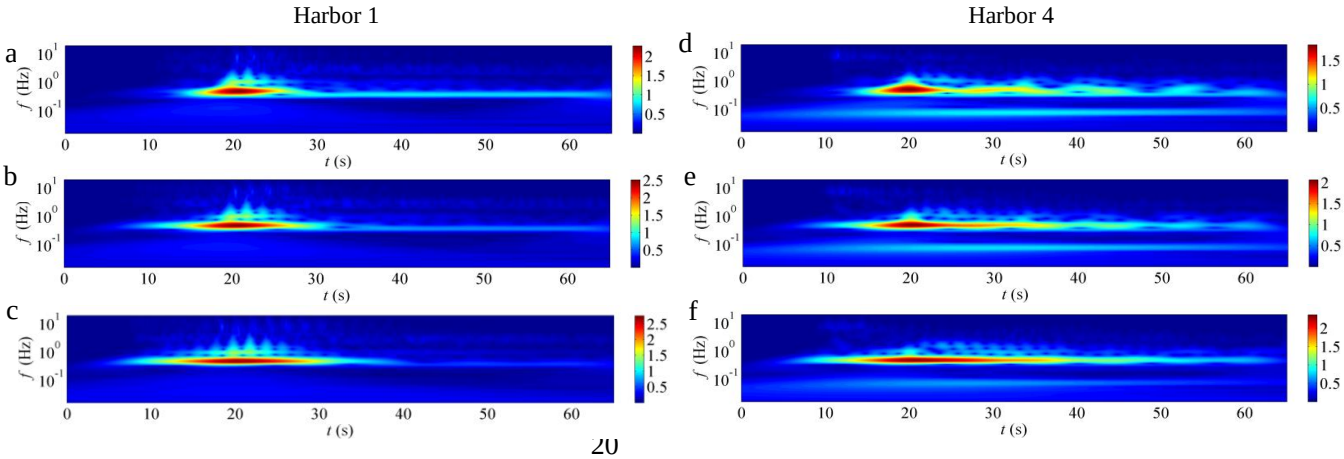

Fig. 12. Wavelet spectra for the time series of the free-surface elevations at gauge G_{01} inside Harbors 1 and 4 presented in Fig. 11. (a)–(c) correspond to Harbor 1 with γ = 1.3, 3.3, and 10, respectively. (d)–(f) correspond to Harbor 4 with γ = 1.3, 3.3, and 10, respectively.

To further verify the above-mentioned inference, the six time-series of the free-surface elevations inside the two harbors shown in Fig. 11 are analyzed by using the MWT technique, and their wavelet spectra are presented in Fig. 12. For the three cases of Harbor 1 (Fig. 12a–c), it is seen that at around the frequency of f = 0.50 Hz, there exists the distinct and persistent wave energy from about t = 10 s to the end of the simulation, which indicates that Mode 1 of Harbor 1 is indeed able to be excited by the focused transient wave groups. For the three cases of Harbor 4 (Fig. 12d–f), the similar phenomenon around f = 0.50 Hz can also be clearly seen. In addition, it can be easily found that at around the frequency of f = 0.083 Hz, there exists persistent wave energy until the end of the simulation as well. These phenomena indicate that for Harbor 4, not only Mode 4 but also Mode 1 are obviously induced by the focused transient wave group (refer to Fig. 7). As mentioned in subsection 3.1, the focused transient wave groups adopted in all numerical experiments are composed of 100 frequency components ranging from $0.3f_p$ to $3.0f_p$ (i.e., from 0.15 Hz to 1.50 Hz). The resonant frequency of $f_{4,1}$ = 0.083 Hz is out of the above frequency range. The reason why the incident focused wave groups can induce Mode 1 of Harbor 4 lies in the nonlinear wave-wave interaction between the primary wave components composing the incident focused wave groups (Chen et al., 2006; Gao et al., 2016; Rogers and Mei, 1978). In fact, Mode 1 of Harbor 3 is also distinctly observed when the harbor is subjected to the focused wave groups with various A_f and γ (not shown here) because of the nonlinear wave-wave interaction.

By adopting the DFT technique to analyze the time series of free-surface elevations at all the numerical wave gauges from t = 10 s to the end of the simulation, the response amplitudes of various resonant modes at different positions inside the harbor can be quantitatively calculated. Further, the resonant modal shape simulated by the numerical model can be obtained by dividing the response amplitude at each wave gauge to that at G_{01}. Fig. 13 illustrates the comparisons of the modal shapes calculated by the analytical solution of Mei (1983) and these predicted by the numerical model for

Mode 1 of Harbor 1, Mode 2 of Harbor 2, Mode 3 of Harbor 3, and Mode 4 of Harbor 4 excited by the normally-incident focused wave groups with A_f = 0.12 m and different values of γ. $A_{i,j}$ and $(A_{i,j})_{G01}$ (i=j=1, 2, 3, and 4) in the figure denote the response amplitudes for Mode j of Harbor i at various positions and at gauge G_{01}, respectively. It is found that for all the twelve cases presented in this figure, the predicted resonant modal shapes coincide fairly well with the analytical ones.

As mentioned above, different from the four modes shown in Fig. 13 which are directly excited by the primary wave components composing the focused wave groups, Mode 1 of Harbor 3 and Mode 1 of Harbor 4 can be triggered via the nonlinear wave-wave interaction between the primary wave components. Furthermore, Fig. 14 shows the comparisons of the modal shapes calculated by the analytical solution of Mei (1983) and these predicted by the numerical model for Mode 1 of Harbor 3 and Mode 1 of Harbor 4. $A_{i,1}$ and $(A_{i,1})_{G01}$ (i=3 and 4) refer to the response amplitudes for Mode 1 of Harbor i at various positions and at gauge G_{01}, respectively. Similar to that shown in Fig. 13, the predicted modal shapes of these two modes also agree well with the analytical ones. It should be noted here that all these phenomena shown in Figs. 12–14 also can be clearly observed inside the four harbors when they are subjected to the parallel-incident wave groups. The corresponding results related to the parallel-incident wave groups are not presented in the article because of space limitations.

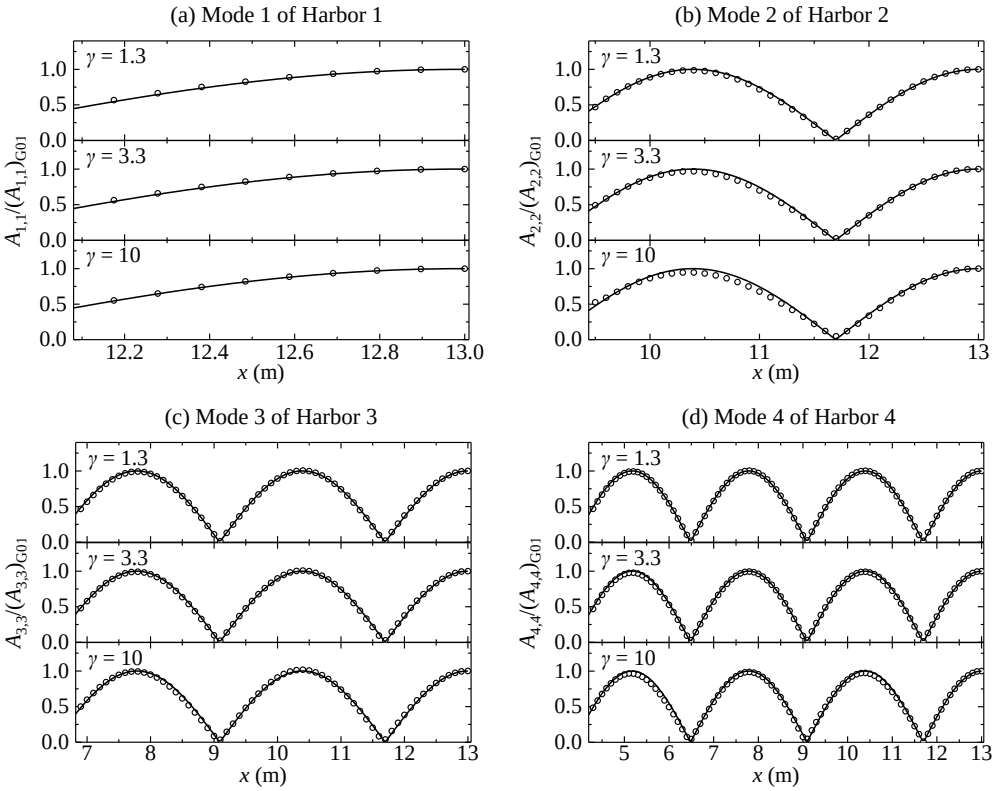

Fig. 13. Analytical modal shapes by Mei (1983)'s solution (lines) and the predicted ones by the numerical model (dots), which are excited by the normally-incident focused wave groups with A_f = 0.12 m and different values of γ. (a)–(d) correspond to Mode 1 of Harbor 1, Mode 2 of Harbor 2, Mode 3 of Harbor 3, and Mode 4 of Harbor 4, respectively. $A_{i,j}$ and $(A_{i,j})_{G01}$ (i=j=1, 2, 3, and 4) refer to the response amplitudes for Mode j of Harbor i at various positions and at gauge G_{01}, respectively.

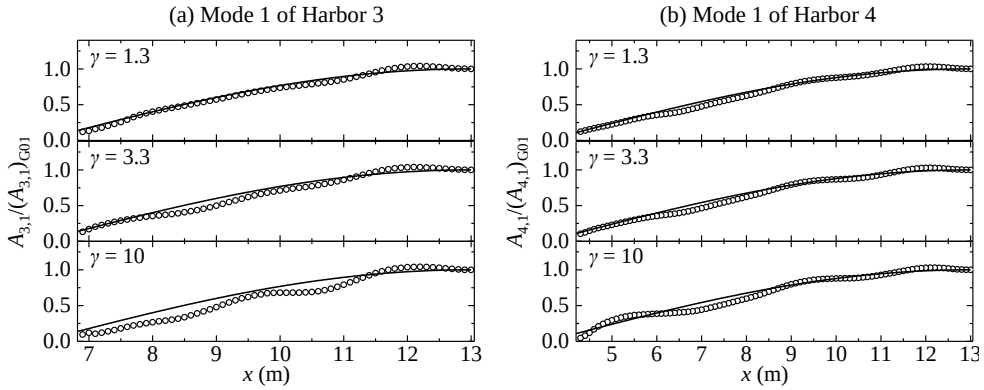

Fig. 14. As in Fig. 13, but (a) and (b) correspond to Mode 1 of Harbor 3 and Mode 1 of Harbor 4, respectively. $A_{i,1}$ and $(A_{i,1})_{G01}$ (i= 3 and 4) refer to the response amplitudes for Mode 1 of Harbor i at various positions and at gauge G_{01}, respectively.

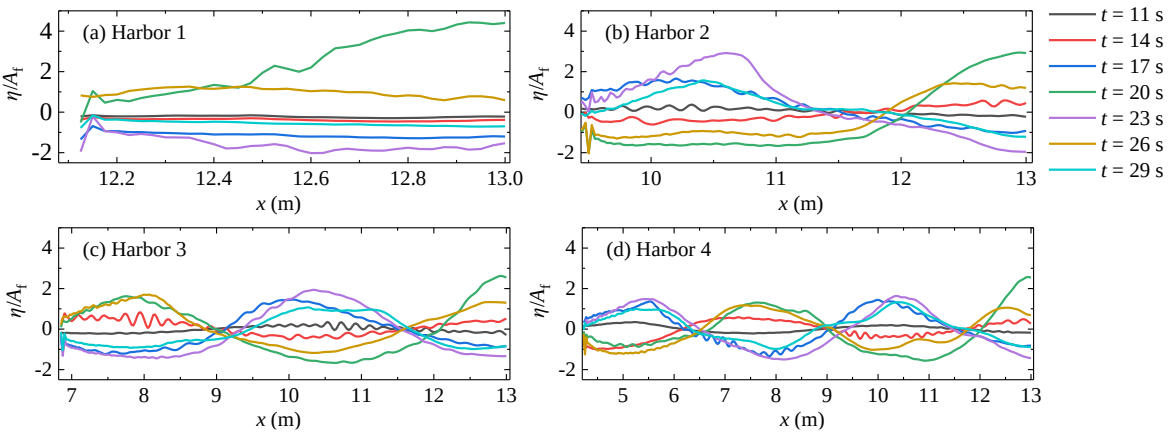

Fig. 15. Evolutions of wave profiles along the central lines of Harbors 1–4 from t=11 s to t=29 s excited by the normally-incident focused wave groups with A_f = 0.12 m and γ =3.3.

To further observe the resonant behavior inside the harbor under the action of focused wave groups, the evolutions of wave profiles along the central lines of Harbors 1–4 from t=11 s to t=29 s excited by the normally-incident focused wave groups with A_f = 0.12 m and γ =3.3 are presented in Fig. 15. It is clearly seen that for all the four harbors considered, the wave surfaces inside them manifest obvious standing wave characteristics. Take Harbors 1 and 4 for example. Inside Harbor 1 (Fig. 15a), there exist an antinode at the backwall and a node near the harbor entrance (i.e., near x=12.08 m). Inside Harbor 4 (Fig. 15d), there exist four antinodes near x=5.5, 8.0, 10.5, and 13.0 m and four nodes near x=4.2, 6.5, 9.0, and 11.8 m. These phenomena indicate that the wave surfaces inside the harbor are dominated mainly by those incident wave components near the spectral peak frequency, and that the incident wave components far away from the spectral peak frequency only play a relatively weak modulation role.

Integrating all the information in both the time- and the frequency-domains presented in Figs. 11–15, it can be concluded that harbor oscillations can be directly induced by the incident focused wave groups when their spectral peak frequency coincides with or approaches one of the resonant frequencies of the harbor. In addition, when the higher resonant modes are directly excited by the incident focused wave groups, the lower resonant modes are also highly likely to be triggered at the same time due to the nonlinear wave energy transfer from the primary wave components to the lower-frequency components.

Owing to the existence of the fully reflected backwall of the harbor, it can be easily observed

from Fig. 13 that the maximum response amplitude for each resonant mode inside the harbor always occurs at the backwall (i.e., at gauge G_{01}). For Mode 1 of Harbor 3 and Mode 1of Harbor 4 shown in Fig. 14, although there exists slightly position deviation from the backwall for the maximum response amplitude, the position deviation is always relatively small and the response amplitude at the backwall is always shown to be extremely close to the maximum one for both modes. Hence, the response amplitude at gauge G_{01} will be selected as the measure of the resonant intensity for each mode in the following sections.

4.2. Effects of the spectral width parameter

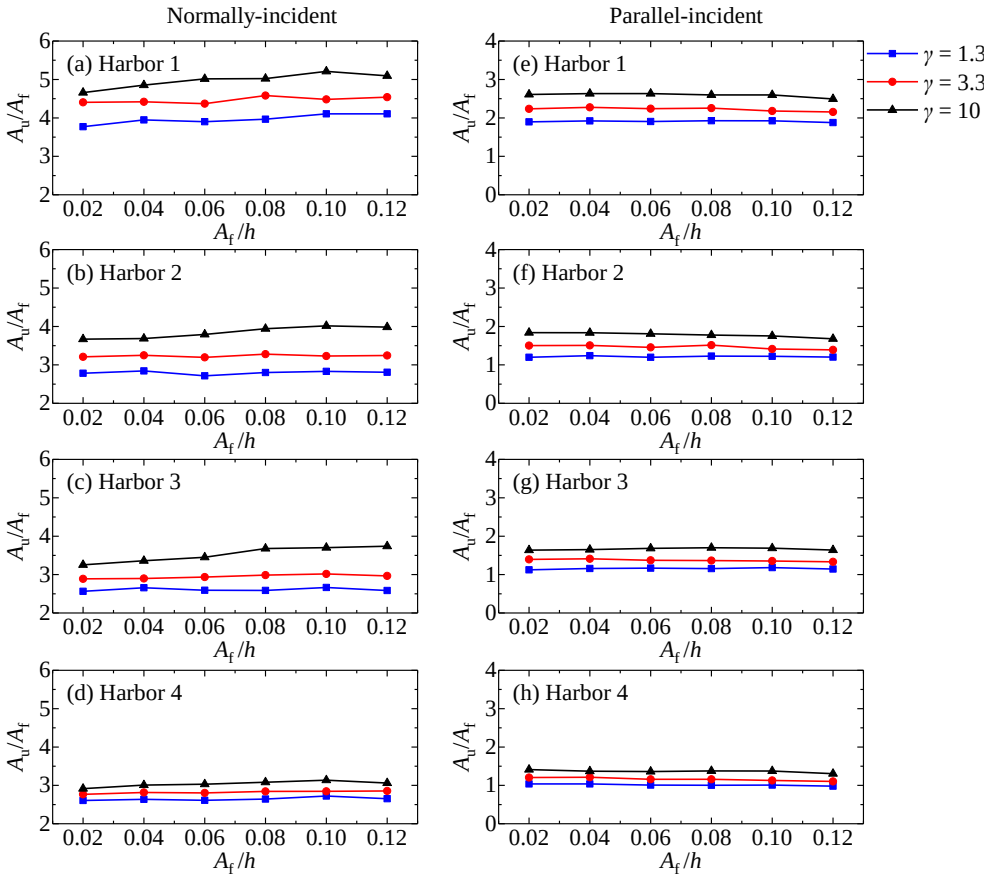

Fig. 16. Maximum runups inside the harbor under the incident focused wave groups with various spectral width parameters γ. (a)–(d) correspond to Harbors 1–4 subjected to normally-incident focused wave groups, respectively. (e)–(h) correspond to Harbors 1–4 subjected to parallel-incident focused wave groups, respectively.

Fig. 16 illustrates the comparisons of the maximum runups inside the harbor under the incident focused wave groups with various spectral width parameters γ. For the normally-incident focused

wave groups (Fig. 16a–d), it is seen that the maximum runups inside all the four harbors are sensitive to the value of γ, and the former is shown to increase gradually with the latter. For the parallel-incident focused wave groups (Fig. 16e–h), the identical phenomenon can also be clearly observed. It can be attributed to different energy spectral structures of the incident focused wave groups with various values of γ. As shown in Fig. 9, the amplitude spectra of the three incident focused wave groups with the same focused wave amplitude presents distinct features. For the amplitude spectrum with γ=1.3 (Fig. 9a), the wave amplitude distribution among the frequency range of $0.3f_p$ and $3.0f_p$ (i.e., between 0.15 Hz and 1.50 Hz) is relatively uniform, and the normalized wave amplitude, A/A_f, at the spectral peak frequency f_p=0.5 Hz is also relatively small. As the value of γ increases, the wave amplitude distribution among the above frequency range becomes increasingly uneven, and an increasing amount of wave energy is concentrated around the spectral peak frequency (Fig. 9b and c). The normalized wave amplitude, A/A_f, at the spectral peak frequency increases from 0.10 to 0.27 when the value of γ rises from 1.3 to 10. Meanwhile, considering that Mode 1 of Harbor 1, Mode 2 of Harbor 2, Mode 3 of Harbor 3 and Mode 4 of Harbor 4 have almost the same linear amplification factor (Fig. 7), the larger wave amplitude at and around the spectral peak frequency will inevitably lead to the larger maximum runup inside the harbor.

Fig. 17 shows the comparisons of the response amplitudes at gauge G_{01} for the four resonant modes that are directly excited by the primary wave components (i.e., Mode 1 of Harbor 1, Mode 2 of Harbor 2, Mode 3 of Harbor 3 and Mode 4 of Harbor 4) under the incident focused wave groups with various spectral width parameters γ. Similar to that shown in Fig. 16, at the variation range of the incident focused wave amplitudes considered, the response amplitudes at gauge G_{01} for all the four resonant modes are also shown to increase gradually with the increase of the spectral width parameters, irrespective of whether the incident focused wave groups propagate into the harbor perpendicularly to or parallel with the harbor entrance. The reason why the resonant intensity for these four modes becomes further strengthened with the increasing of γ can also be attributed to the distinct amplitude spectral features of the incident focused wave groups with various values of γ and their almost equal linear amplification factors.

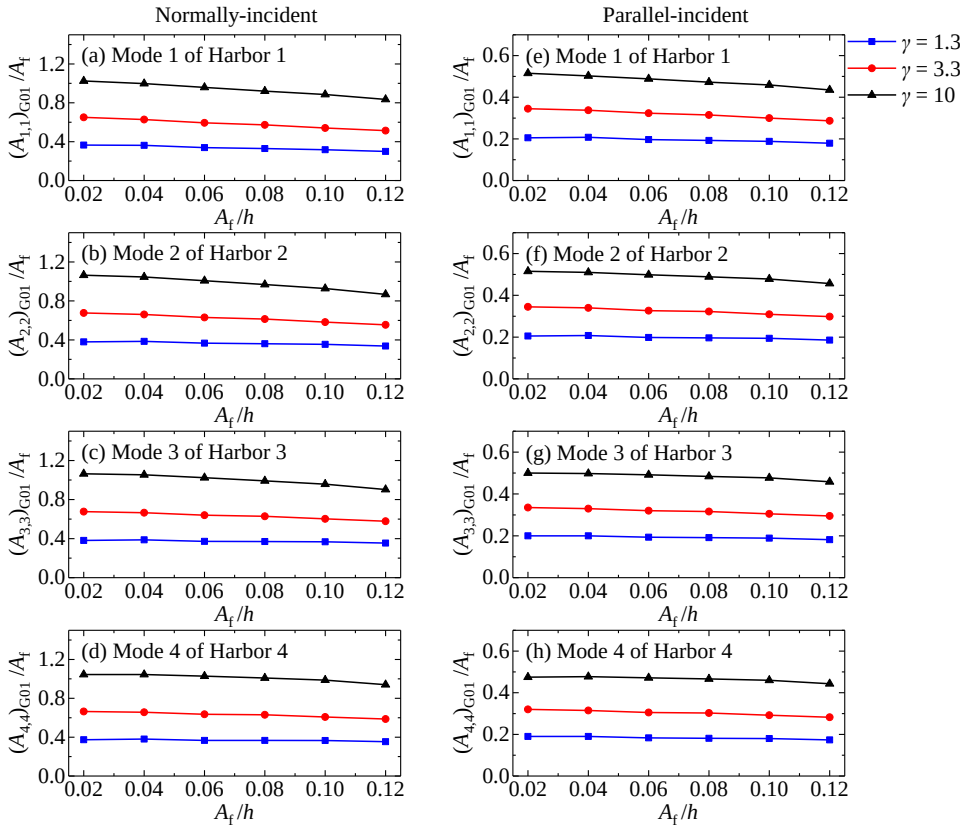

Fig. 17. Response amplitudes at gauge G_{01} for certain resonant modes under the incident focused wave groups with various spectral width parameters γ. (a)–(d) correspond to Mode 1 of Harbor 1, Mode 2 of Harbor 2, Mode 3 of Harbor 3, and Mode 4 of Harbor 4, excited by normally-incident focused wave groups, respectively. (e)–(h) correspond to the four modes excited by parallel-incident focused wave groups, respectively.

Fig. 18 further presents the comparisons of the response amplitudes at gauge G_{01} for the two resonant modes that are triggered via the nonlinear wave-wave interaction between the primary wave components (i.e., Mode 1 of Harbor 3 and Mode 1 of Harbor 4) under the incident focused wave groups with various spectral width parameters γ. Different from the phenomenon shown in Fig. 17, the influences of the spectral width parameter on the resonant intensity for the two modes generated by the nonlinear wave-wave interaction depend on the specific harbor. For Mode 1 of Harbor 3, the response amplitudes at gauge G_{01} is shown to gradually decrease with the increase of the spectral width parameter, irrespective of the incident wave direction. However, for Mode 1 of Harbor 4, the resonant intensity inside the harbor does not monotonically vary with the spectral width parameter anymore. The values of γ = 3.3 and 10 always produces the largest and the smallest

response amplitudes at gauge G_{01}, respectively.

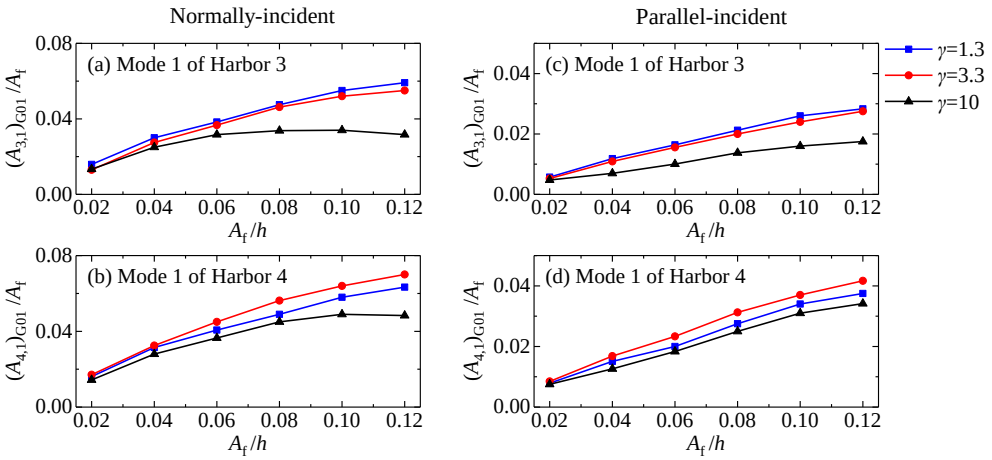

Fig. 18. As in Fig. 17, but (a) and (b) correspond to Mode 1 of Harbor 3 and Mode 1 of Harbor 4, excited by normally-incident focused wave groups, respectively. (c) and (d) correspond to the two modes excited by parallel-incident focused wave groups, respectively.

4.3. Effects of the incident wave direction

Fig. 19 shows the comparisons of the maximum runups inside Harbors 1–4 subjected to focused transient wave groups with different incident directions. It is observed that for all four harbors, the maximum runups excited by the normally-incident focused wave groups are always significantly larger than those induced by the corresponding parallel-incident focused wave groups, irrespective of the spectral width parameter. This is mainly because when the normally-incident focused wave groups are fully reflected at the backwall of the harbor, and the wave amplitude at gauge G_{01} will be amplified by roughly twice under this case. However, under the parallel-incident wave conditions, the incident wave direction is parallel with the backwall of the harbor. The magnification effect caused by the fully reflection of the backwall no longer exists. To further validate these explanations, the ratios of the maximum runup excited by the normally-incident waves and the corresponding one triggered by the parallel-incident waves for all four harbors and all three spectral width parameters are calculated, and it can be found that the ratio of the maximum runup for all these cases varies between 1.8 and 2.7 (i.e., the ratio always fluctuates around 2.0), which fully proves the above explanations.

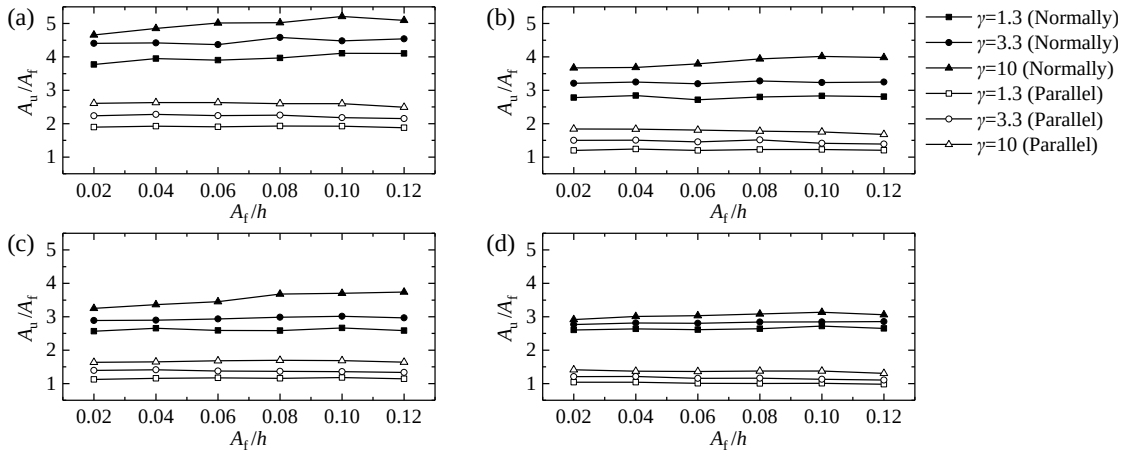

Fig. 19. Comparisons of the maximum runups inside the harbor under the normally- and parallel-incident focused wave groups. (a)–(d) correspond to Harbors 1–4, respectively.

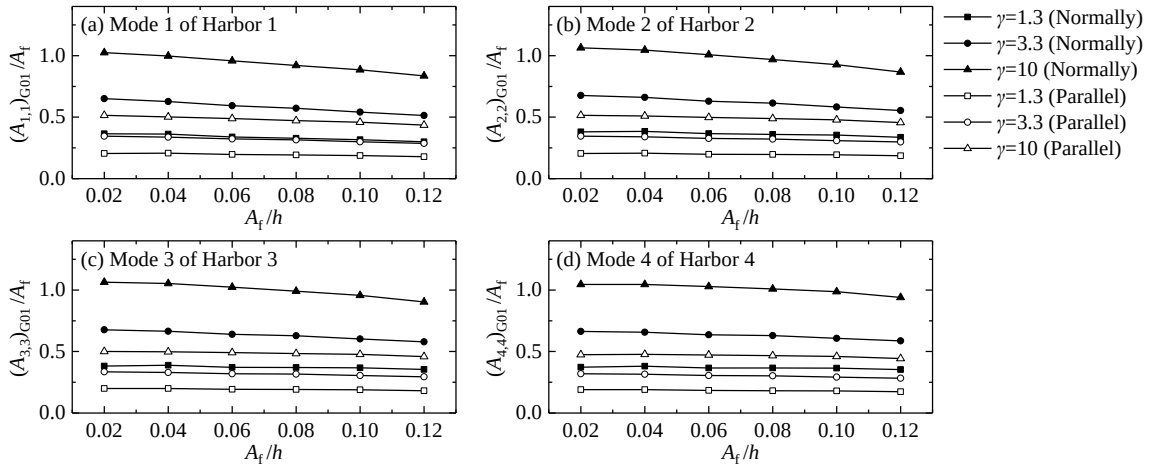

Fig. 20. Comparisons of the response amplitudes at gauge G_{01} for certain resonant modes under the normally- and parallel-incident focused wave groups. (a)–(d) correspond to Mode 1 of Harbor 1, Mode 2 of Harbor 2, Mode 3 of Harbor 3, and Mode 4 of Harbor 4, respectively.

Fig. 20 illustrates the comparisons of the response amplitudes at gauge G_{01} for Mode 1 of Harbor 1, Mode 2 of Harbor 2, Mode 3 of Harbor 3, and Mode 4 of Harbor 4 under the focused wave groups with different incident directions. Similar to that shown in Fig. 19, the resonant intensity excited by the normally-incident focused wave groups are always significantly larger than those induced by the corresponding parallel-incident focused wave groups. By further calculating the ratios of the response amplitudes at gauge G_{01} excited by the normally-incident waves and the corresponding one triggered by the parallel-incident waves for all four harbors and all three spectral

width parameters, it is observed that the ratio of the response amplitude for all these cases varies from 1.7 to 2.2. This indicates that the difference of the response amplitudes shown in this figure can also be ascribed to the reason described in the above paragraph.

Fig. 21 further presents the comparisons of the response amplitudes at gauge G_{01} for Mode 1 of Harbor 3 and Mode 1 of Harbor 4 under the focused wave groups with different incident directions. Phenomenon similar to that shown in Fig. 20 is also clearly observed, and the ratio of the response amplitude under the normally- and parallel-incident wave conditions for these two resonant modes varies between 1.4 and 3.6.

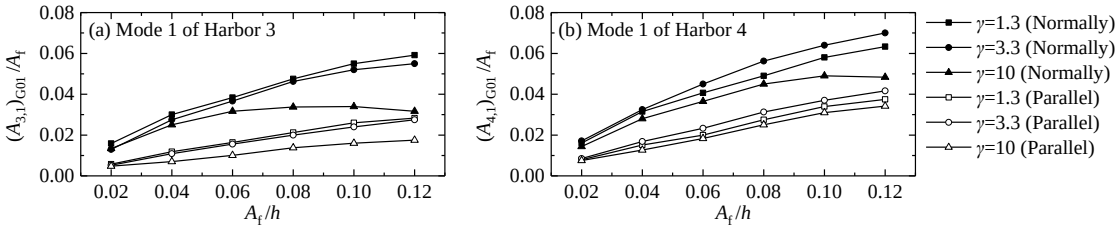

Fig. 21. As in Fig. 20, but (a) and (b) correspond to Mode 1 of Harbor 3 and Mode 1 of Harbor 4, respectively.

4.4. Effects of different resonant modes

Fig. 22 shows the comparisons of the maximum runups inside Harbors 1–4. There are two obvious phenomena that can be observed from this figure. First, the maximum runup inside the harbor gradually decreases from Harbor 1 to Harbor 4, irrespective of the value of γ and incident wave direction, except that under the condition of the normally-incident wave groups with γ=1.3 and larger focused wave amplitudes (Fig. 22a), the maximum runup inside Harbor 4 is slightly larger than that inside Harbor 3. Second, the maximum runups inside Harbor 1 are shown to be significantly larger than those inside the other three harbors. Compared to the difference of the maximum runups between Harbor 1 and Harbors 2–4, the difference between the maximum runups among Harbors 2–4 is obviously smaller, and the smaller the value of γ is, the more pronounced this phenomenon becomes.

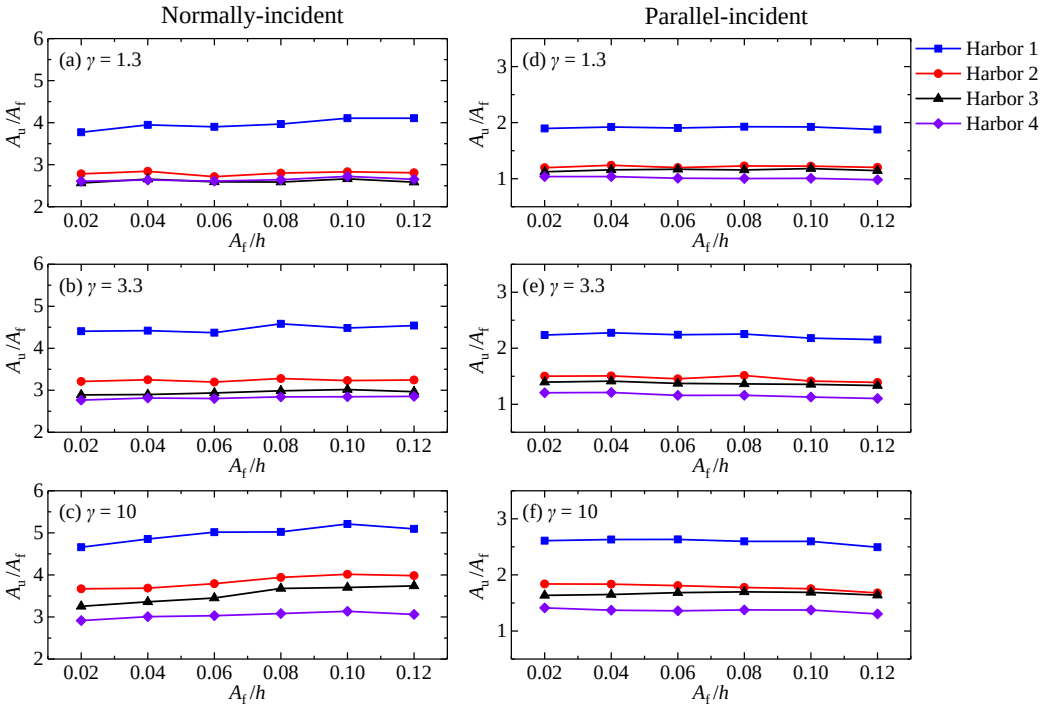

Fig. 22. Comparisons of the maximum runups inside Harbors 1-4. (a)–(c) and (d)–(f) correspond to the normally- and parallel-incident focused wave groups, respectively.

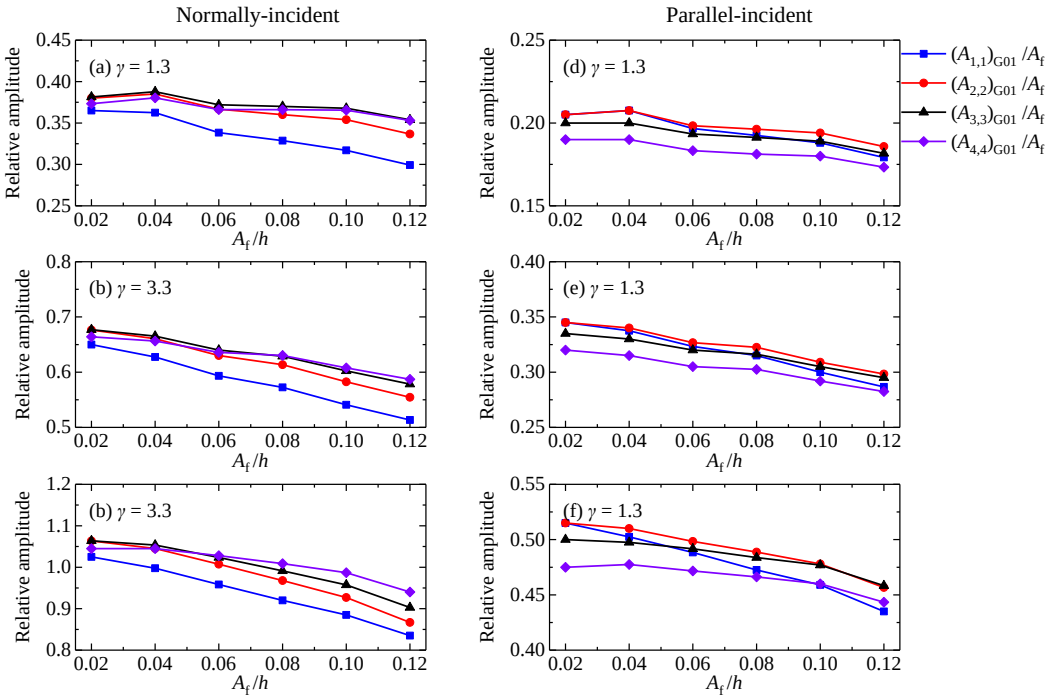

Fig. 23. Comparisons of the response amplitudes at gauge G_{01} between Mode 1 of Harbor 1, Mode 2 of Harbor 2, Mode 3 of Harbor 3, and Mode 4 of Harbor 4. (a)–(c) and (d)–(f) correspond to the normally- and parallel-incident focused wave groups, respectively.

Fig. 23 shows the comparisons of the response amplitudes at gauge G_{01} between Mode 1 of Harbor 1, Mode 2 of Harbor 2, Mode 3 of Harbor 3, and Mode 4 of Harbor 4. It is observed that for these four modes that are directly triggered by the primary wave components, the effects of different modes on the resonant intensity inside the harbor depend closely on the incident wave direction. Under the normally-incident wave conditions (Fig. 23a–c), Mode 1 of Harbor 1 always has the smallest resonant intensity among the four resonant modes, irrespective of the spectral width parameter. However, the largest resonant intensity among the four resonant modes depends on the incident focused wave amplitude. When the incident focused wave amplitude is small, the largest resonant intensity tends to occur in Mode 3 of Harbor 3. As the former increases, the latter tends to occur in Mode 4 of Harbor 4. Under parallel-incident wave conditions (Fig. 23d–f), the smallest and largest resonant intensities always occur in Mode 4 of Harbor 4 and Mode 2 of Harbor 2, respectively.

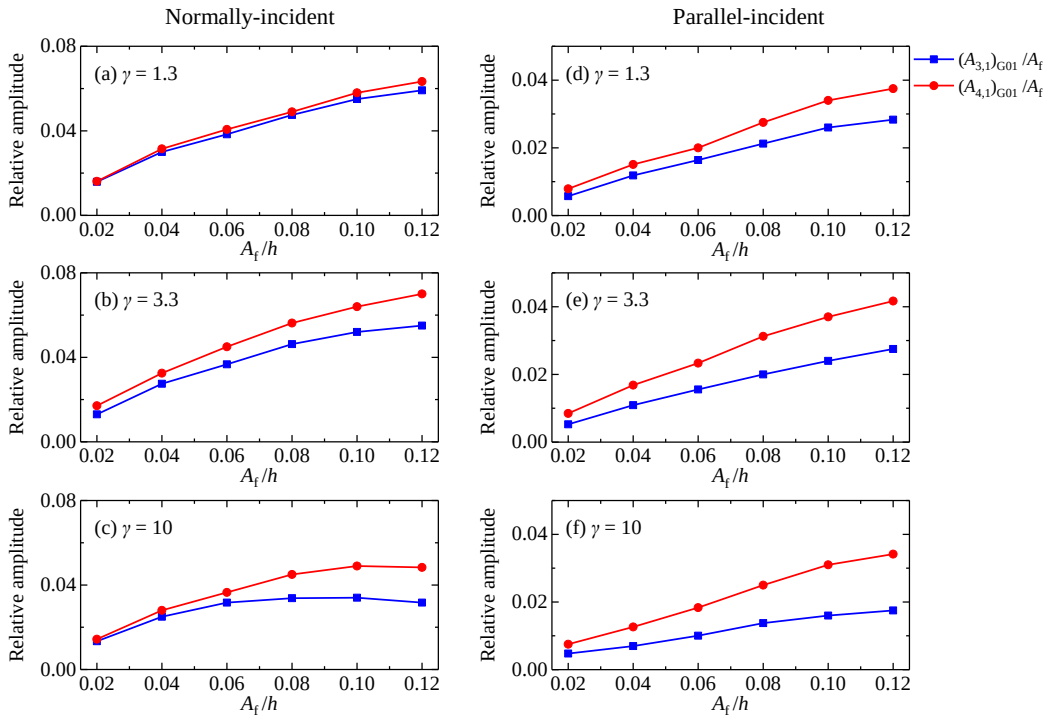

Fig. 24. Comparisons of the response amplitudes at gauge G_{01} between Mode 1 of Harbor 3 and Mode 1 of Harbor 4. (a)–(c) and (d)–(f) correspond to the normally- and parallel-incident focused wave groups, respectively..

Fig. 24 further presents the comparisons of the response amplitudes at gauge G_{01} between Mode 1 of Harbor 3 and Mode 1 of Harbor 4. It can be clearly seen that the resonant intensity for

Mode 1 of Harbor 4 is always larger than the corresponding one for Mode 1 of Harbor 3, irrespective of the spectral width parameter and incident wave direction. This is probably because the linear amplification factor of Mode 1 of Harbor 4 is obviously larger than that of Mode 1 of Harbor 3 (refer to Fig. 7).

5. Conclusions

In this study, the interactions between four elongated rectangular harbors (Harbors 1–4) and focused transient wave groups are investigated by using the fully nonlinear Boussinesq model, FUNWAVE 2.0, for the first time. The focused transient wave groups with various focused wave amplitudes, spectral width parameters, and incident directions are considered, and all of them have the identical spectral peak frequency of f_p=0.50 Hz, which is equal to the resonant frequency of Mode 1 of Harbor 1, Mode 2 of Harbor 2, Mode 3 of Harbor 3, and Mode 4 of Harbor 4. Based on the linear wave theory and the iterative approach for correcting both the focused wave amplitude and focused phase, the desired focused wave groups are accurately generated by the numerical model. Further, both the time- and frequency-domain information of the wave surfaces inside the harbor is analyzed using the MWT and DFT techniques. The capability of the focused transient wave groups to trigger harbor resonance is revealed first; the effects of the spectral width parameter, incident wave direction, and resonant mode on maximum runup and response intensity inside the harbor are comprehensively investigated subsequently. The results of this study will expand the knowledge of the harbor oscillations induced by extreme wave conditions.

The following conclusions can be drawn from the results of this study:

1. By checking the wavelet spectra of the wave surfaces and comparing the analytical and numerical-predicted modal structures inside the harbor, it is found for the first time that the focused wave groups can directly excite harbor resonance when their spectral peak frequency equals or approaches one of the resonant frequencies of the harbor. In addition, when the higher resonant modes are directly excited by the incident focused wave groups, the lower resonant modes are also highly likely to be triggered at the same time because of the nonlinear wave-wave interaction that can transfer the wave energy from the primary wave components to the lower-frequency components.
2. Both maximum runup and resonant intensity inside the harbor are significantly affected by the

spectral width parameters. Both the maximum runups inside all the four harbors and the resonant intensities for the resonant modes directly excited by the primary wave components (i.e., Mode 1 of Harbor 1, Mode 2 of Harbor 2, Mode 3 of Harbor 3 and Mode 4 of Harbor 4) are observed to increase gradually with the increase of the spectral width parameter. However, for the resonant intensities for the modes induced by nonlinear wave-wave interaction (i.e., Mode 1 of Harbor 3 and Mode 1 of Harbor 4), the influences of the spectral width parameter on their resonant intensities depend on the specific harbor.

3. Incident wave direction has also dramatic effects on maximum runup and resonant intensity inside the harbor. For all the four harbors, both the maximum runup and the resonant intensity excited by the normally-incident focused wave groups are shown to be significantly larger than those induced by the corresponding parallel-incident focused wave groups, irrespective of the spectral width parameter and whether the resonant modes are triggered directly by the primary wave components or by the nonlinear wave-wave interaction.
4. Maximum runup and resonant intensity inside the harbor are also sensitive to the resonant modes. The maximum runup inside the harbor is observed to decrease gradually from Harbor 1 to Harbor 4 overall, irrespective of the value of γ and incident wave direction. For the four modes that are directly triggered by the primary wave components, the effects of different modes on the resonant intensity inside the harbor depend closely on the incident wave direction. For the two resonant modes induced by nonlinear wave-wave interaction, the resonant intensity for Mode 1 of Harbor 4 is always larger than the corresponding one for Mode 1 of Harbor 3, irrespective of the spectral width parameter and incident wave direction.

Finally, we reaffirm that these conclusions are only valid for the given harbors with constant depth, the given resonant modes, and the variation ranges of the incident focused wave amplitude, spectral width parameter, and incident wave direction considered in this study.

Acknowledgments

This study was financially supported by the National Key Research and Development Program (2017YFC1404200), the National Natural Science Foundation of China (Grant Nos. 51911530205, 51609108, 51709136 and 51679113), the Royal Society of UK (Grant No. IEC\NSFC\181321), the

Jiangsu Government Scholarship for Overseas Studies (awarded to Dr. Junliang Gao for study abroad at the University of Bath), the Natural Science Foundation of Jiangsu Province of China (Grant No. BK20170576), and the Natural Science Research of Jiangsu Higher Education Institutions of China (Grant No. 17KJB580006).

References

Baldock, T.E., Swan, C., Taylor, P.H., 1996. A laboratory study of nonlinear surface waves on water. Philosophical Transactions: Mathematical, Physical and Engineering Sciences 354 (1707), 649-676.

Bellotti, G., 2007. Transient response of harbours to long waves under resonance conditions. Coastal Engineering 54 (9), 680-693.

Bowers, E.C., 1977. Harbour resonance due to set-down beneath wave groups. Journal of Fluid Mechanics 79, 71-92.

Bredmose, H., Jacobsen, N.G., 2010. Breaking Wave Impacts on Offshore Wind Turbine Foundations: Focused Wave Groups and CFD, the ASME 2010 29th International Conference on Ocean, Offshore and Arctic Engineering, Shanghai, China, pp. OMAE2010-20368.

Bruno, D., Serio, F.D., Mossa, M., 2009. The FUNWAVE model application and its validation using laboratory data. Coastal Engineering 56 (7), 773-787.

Buldakov, E.V., Taylor, R.E., Taylor, P.H., 2003. Diffraction of a directionally spread wave group by a cylinder. Applied Ocean Research 25 (6), 301-320.

Chawla, A., Kirby, J.T., 2000. A source function method for generation of waves on currents in Boussinesq models Applied Ocean Research 22 (2), 75-83.

Chen, L.F., Zang, J., Taylor, P.H., Sun, L., Morgan, G.C.J., Grice, J., Orszaghova, J., Ruiz, M.T., 2018. An experimental decomposition of nonlinear forces on a surface-piercing column: Stokes-type expansions of the force harmonics. Journal of Fluid Mechanics 848, 42-77.

Chen, M.-Y., Mei, C.C., Chang, C.-K., 2006. Low-frequency spectra in a harbour excited by short and random incident waves. Journal of Fluid Mechanics 563, 261-281.

De Girolamo, P., 1996. An experiment on harbour resonance induced by incident regular waves and irregular short waves. Coastal Engineering 27, 47-66.

De Jong, M.P.C., Battjes, J.A., 2004. Seiche characteristics of Rotterdam Harbour. Coastal

Engineering 51 (5-6), 373-386.

Dong, G.-H., Ma, Y.-X., Ma, X.-Z., 2008. Cross-shore variations of wave groupiness by wavelet transform. Ocean Engineering 35 (7), 676-684.

Dong, G., Gao, J., Ma, X., Wang, G., Ma, Y., 2013. Numerical study of low-frequency waves during harbor resonance. Ocean Engineering 68, 38-46.

Dong, G., Liu, D., Ma, Y., Perlin, M., 2019. Experimental investigation of weakly three-dimensional nonlinear wave interactions. European Journal of Mechanics / B Fluids 77, 239-251.

Dong, G., Wang, G., Ma, X., Ma, Y., 2010a. Harbor resonance induced by subaerial landslide-generated impact waves. Ocean Engineering 37 (10), 927-934.

Dong, G., Wang, G., Ma, X., Ma, Y., 2010b. Numerical study of transient nonlinear harbor resonance. Science China-Technological Sciences 53, 558-565.

Fabrikant, A.L., 1995. Harbor oscillations generated by shear flow. Journal of Fluid Mechanics 282, 203-217.

Fernández, H., Sriram, V., Schimmels, S., Oumeracic, H., 2014. Extreme wave generation using self correcting method - Revisited. Coastal Engineering 93, 15-31.

Gao, J., Ji, C., Gaidai, O., Liu, Y., 2016. Numerical study of infragravity waves amplification during harbor resonance. Ocean Engineering 116, 90-100.

Gao, J., Ji, C., Gaidai, O., Liu, Y., Ma, X., 2017a. Numerical investigation of transient harbor oscillations induced by N-waves. Coastal Engineering 125, 119-131.

Gao, J., Ji, C., Liu, Y., Ma, X., Gaidai, O., 2017b. Influence of offshore topography on the amplification of infragravity oscillations within a harbor. Applied Ocean Research 65, 129-141.

Gao, J., Ji, C., Liu, Y., Ma, X., Gaidai, O., 2018a. Numerical study on transient harbor oscillations induced by successive solitary waves. Ocean Dynamics 68 (2), 193-209.

Gao, J., Ma, X., Dong, G., Zang, J., Zhou, X., Zhou, L., 2019a. Topographic influences on transient harbor oscillations excited by N-waves. Ocean Engineering 192, 106548.

Gao, J., Zhou, X., Zang, J., Chen, Q., Zhou, L., 2018b. Influence of offshore fringing reefs on infragravity period oscillations within a harbor. Ocean Engineering 158, 286-298.

Gao, J., Zhou, X., Zhou, L., Zang, J., Chen, H., 2019b. Numerical investigation on effects of fringing reefs on low-frequency oscillations within a harbor. Ocean Engineering 172, 86-95.

Goda, Y., 1999. A comparative review on the functional forms of directional wave spectrum. Coastal

Engineering Journal 41 (1), 1–20.

Goupillaud, P., Grossmann, A., Morlet, J., 1984. Cycle-octave and related tranforms in seismic signal analysis. Geoexploration Amsterdam 23 (1), 85–102.

Gulshan, Kumar, P., Rajni, 2020. Moored ship motion analysis in Paradip port under the resonance conditions using 3-D boundary element method. Journal of Marine Science and Technology, https://doi.org/10.1007/s00773-020-00701-0.

Huang, M.C., 2004. Wave parameters and functions in wavelet analysis. Ocean Engineering 31, 111–125.

Hunt-Raby, A.C., Borthwick, A.G.L., Stansby, P.K., Taylor, P.H., 2011. Experimental measurement of focused wave group and solitary wave overtopping. Journal of Hydraulic Research 49 (4), 450-464.

Johannessen, T.B., Swan, C., 2008. A laboratory study of the focusing of transient and directionally spread surface water waves. Royal Society of London Proceedings Series A 457, 971-1006.

Jonathan, P., Taylor, P.H., 1997. On irregular, nonlinear waves in a spread sea. Journal of Offshore Mechanics and Arctic Engineering 119 (1), 37-41.

Judge, F.M., Hunt-Raby, A.C., Orszaghova, J., Taylor, P.H., Borthwickd, A.G.L., 2019. Multi-directional focused wave group interactions with a plane beach. Coastal Engineering 152, 103531.

Kennedy, A.B., Kirby, J.T., Chen, Q., Dalrymple, R.A., 2001. Boussinesq-type equations with improved nonlinear performance. Wave Motion 33, 225-243.

Kirby, J.T., Long, W., Shi, F., 2003. Funwave 2.0 Fully Nonlinear Boussinesq Wave Model On Curvilinear Coordinates. Report No. CACR-02-xx. Center for Applied Coastal Research, Dept. of Civil & Environmental Engineering, University of Delaware, Newark, Delaware.

Kumar, P., Gulshan, 2017. Extreme wave-induced oscillation in Paradip Port under the resonance conditions. Pure and Applied Geophysics 174 (2), 4501-4516.

Kumar, P., Gulshan, 2018. Theoretical analysis of extreme wave oscillation in Paradip Port using a 3-D boundary element method. Ocean Engineering 164, 13-22.

Kumar, P., Zhang, H., Kim, K.I., Yuen, D.A., 2016. Modeling wave and spectral characteristics of moored ship motion in Pohang New Harbor under the resonance conditions. Ocean Engineering 119, 101-113.

López, M., Iglesias, G., 2014. Long wave effects on a vessel at berth. Applied Ocean Research 47, 63-72.

Lee, C., Cho, Y.-S., Yum, K., 2001. Internal generation of waves for extended Boussinesq equations. Coastal Engineering 42, 115-162.

Lindgren, G., 1970. Some properties of a normal process near a local maximum. The Annals of Mathematical Statistics 41 (6), 1870-1883.

Liu, D., Ma, Y., Dong, G., Perlin, M., 2015. An experimental study of weakly three-dimensional non-breaking and breaking waves. European Journal of Mechanics - B/Fluids 52, 206-216.

Liu, P.L.-F., Monserrat, S., Marcos, M., Rabinovich, A.B., 2003. Coupling between two inlets: Observation and modeling. Journal of Geophysical Research: Oceans 108, C3, 3069, doi:10.1029/2002JC001478.

Losada, I.J., Gonzalez-Ondina, J.M., Diaz-Hernandez, G., Gonzalez, E.M., 2008. Numerical modeling of nonlinear resonance of semi-enclosed water bodies: Description and experimental validation. Coastal Engineering 55, 21-34.

Ma, Y., Dong, G., Perlin, M., Liu, S., Zang, J., Sun, Y., 2009. Higher-harmonic focused-wave forces on a vertical cylinder. Ocean Engineering 36, 595-604.

Marcos, M., Liu, P.L.-F., Monserrat, S., 2004. Nonlinear resonant coupling between two adjacent bays. Journal of Geophysical Research: Oceans 109, C05008, doi:10.1029/2003JC002039.

Mei, C.C., 1983. The Applied Dynamics of Ocean Surface Waves. Wiley, New York.

Miles, J.W., 1974. Harbor seiching. Annual Review of Fluid Mechanics 6, 17-33.

Nikolkina, I., Didenkulova, I., 2011. Rogue waves in 2006–2010. Natural Hazards and Earth System Sciences 11, 2913–2924.

Ning, D., Wang, R., Chen, L., Li, J., Zang, J., Cheng, L., Liu, S., 2017. Extreme wave run-up and pressure on a vertical seawall. Applied Ocean Research 67, 188-200.

Okihiro, M., Guza, R.T., 1996. Observations of seiche forcing and amplification in three small harbors. Journal of Waterway, Port, Coastal and Ocean Engineering 122 (5), 232-238.

Paulsen, B.T., Bredmose, H., Bingham, H.B., 2014. An efficient domain decomposition strategy for wave loads on surface piercing circular cylinders. Coastal Engineering 86, 57-76.

Rabinovich, A.B., 2009. Seiches and harbor oscillations, in: Kim, Y. (Ed.), Handbook of Coastal and Ocean Engineering. World Scientific Publishing, Singapore, pp. 193-236.

Rogers, S.R., Mei, C.C., 1978. Nonlinear resonant excitation of a long and narrow bay. Journal of Fluid Mechanics 88 (1), 161-180.

Rupali, Kumar, P., Rajni, 2020. Spectral boundary element modeling of water waves in Pohang New Harbor and Paradip Port. Ocean Engineering 196, 106765.

Schmittner, C., Kosleck, S., Hennig, J., 2009. A phase-amplitude iteration scheme for the optimization of deterministic wave sequences, Proceedings of the 28th International Conference on Ocean, Offshore and Arctic Engineering, Honolulu, Hawaii, USA. Paper No. OMAE2009-80131.

Tromans, P.S., Anaturk, A.R., Hagemeijer, P., 1991. A new model for the kinematics of large ocean waves - application as a design wave, The First International Offshore and Polar Engineering Conference. International Society of Offshore and Polar Engineers (ISOPE), Edinburgh.

Vanoni, V.A., Carr, J.H., 1950. Harbor surging, Proceedings of the 1st International Conference on Coastal Engineering, Long Beach, pp. 60-68.

Wang, G., Dong, G., Perlin, M., Ma, X., Ma, Y., 2011. An analytic investigation of oscillations within a harbor of constant slope. Ocean Engineering 38, 479-486.

Wang, G., Zheng, J., Liang, Q., Zheng, Y., 2014. Analytical solutions for oscillations in a harbor with a hyperbolic-cosine squared bottom. Ocean Engineering 83, 16-23.

Wei, G., Kirby, J.T., Grilli, S.T., Subramanya, R., 1995. A fully nonlinear Boussinesq model for surface waves. Part 1. Highly nonlinear unsteady waves. Journal of Fluid Mechanics 294, 71-92.

Zhao, W., Wolgamot, H.A., Taylor, P.H., Taylor, R.E., 2017. Gap resonance and higher harmonics driven by focused transient wave groups. Journal of Fluid Mechanics 812, 905-939.